Cell Systems

Article

Macrophage memory emerges from coordinated transcription factor and chromatin dynamics

Graphical abstract

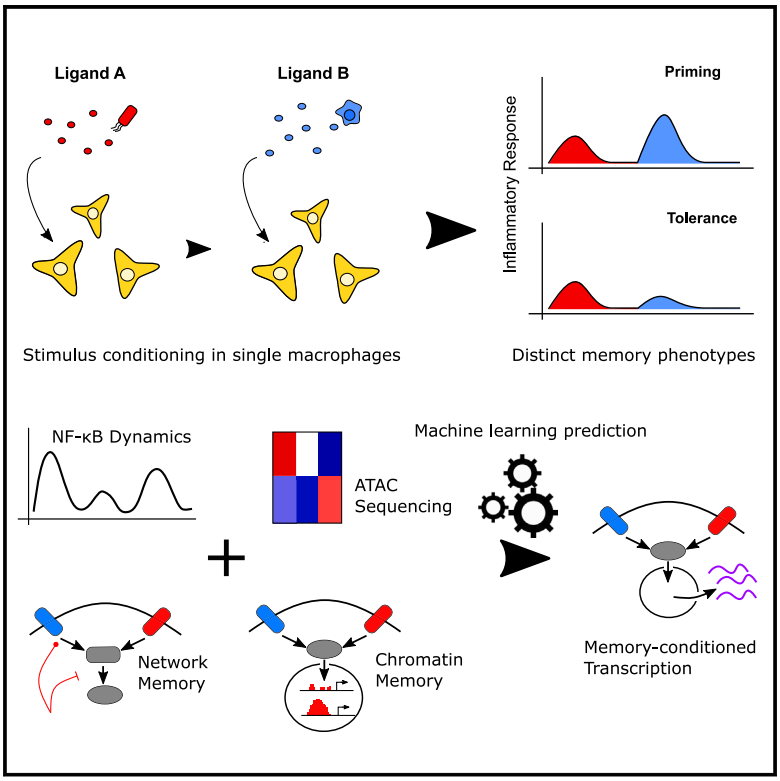

Authors

Andrew G. Wang, Minjun Son, Aleksandr Gorin, ..., Adam Schauer, Alexander Hoffmann, Savaş Tay

Correspondence

tays@uchicago.edu

In brief

Wang et al. combine microfluidic live-cell imaging, chromatin accessibility measurements, and transcriptomics to study how memory is encoded in macrophages. NF-κB activation and chromatin accessibility dynamics each encode unique aspects of prior inflammatory stimulus. Combining information from these sources into a deep-learning model accurately predicts the transcriptional response following re-stimulus.

Highlights

- Macrophages encode memory in NF-κB activation and chromatin accessibility dynamics
- Information on prior stimuli is encoded in individual macrophages
- *In vivo* systemic inflammation reshapes NF-κB activation dynamics in adult macrophages
- Deep learning on NF-κB and chromatin features predicts memory-conditioned transcription

Wang et al., 2025, Cell Systems *16*, 101171
February 19, 2025
https://doi.org/10.1016/j.cels.2025.101171

CellPress

Cell Systems

CellPress

Article

Macrophage memory emerges from coordinated transcription factor and chromatin dynamics

Andrew G. Wang,[1,2,6] Minjun Son,[1,3,6] Aleksandr Gorin,[4] Emma Kenna,[1] Abinash Padhi,[1] Bijentimala Keisham,[1] Adam Schauer,[3] Alexander Hoffmann,[5] and Savaş Tay[1,7,*]

[1]Pritzker School of Molecular Engineering, University of Chicago, Chicago, IL 60637, USA
[2]Medical Scientist Training Program, University of Chicago, Chicago, IL 60637, USA
[3]Chan Zuckerberg Biohub Chicago, Chicago, IL, USA
[4]Department of Medicine, Division of Infectious Diseases, University of California, Los Angeles, Los Angeles, CA 90095, USA
[5]Department of Microbiology, Immunology and Molecular Genetics, University of California, Los Angeles, Los Angeles, CA 90095, USA
[6]These authors contributed equally
[7]Lead contact
*Correspondence: tays@uchicago.edu
https://doi.org/10.1016/j.cels.2025.101171

SUMMARY

Cells of the immune system operate in dynamic microenvironments where the timing, concentration, and order of signaling molecules constantly change. Despite this complexity, immune cells manage to communicate accurately and control inflammation and infection. It is unclear how these dynamic signals are encoded and decoded and if individual cells retain the memory of past exposure to inflammatory molecules. Here, we use live-cell analysis, ATAC sequencing, and an *in vivo* model of sepsis to show that sequential inflammatory signals induce memory in individual macrophages through reprogramming the nuclear factor κB (NF-κB) network and the chromatin accessibility landscape. We use transcriptomic profiling and deep learning to show that transcription factor and chromatin dynamics coordinate fine-tuned macrophage responses to new inflammatory signals. This work demonstrates how macrophages retain the memory of previous signals despite single-cell variability and elucidates the mechanisms of signal-induced memory in dynamic inflammatory conditions like sepsis.

INTRODUCTION

Cells are exposed to combinations of time-varying signaling inputs in their native microenvironments. These signals coordinate fundamental processes in immunity, development, maintenance of homeostasis, and tissue repair.[1,2] The combination, order, and duration of signaling inputs provide cells the information about appropriate transcriptional responses.[3,4] For example, acute inflammation triggered by infection or injury arises from the coordinated processing of signals from pathogens, pro-inflammatory cytokines, and anti-inflammatory molecules, spanning durations from hours to days.[3] The correct sequence of ligand exposure and receptor stimulation results in an appropriately transient pro-inflammatory response that clears the infection but limits damage to cells or tissues, followed by secretion of anti-inflammatory and tissue repair molecules. However, incorrect stimulation sequence can produce chronic infection or excessive tissue damage and autoimmunity.[5–7] Interestingly, a large number of extracellular signals converge on a limited number of information-processing pathways and share intracellular components. How cells utilize such limited information-processing machinery to integrate diverse and dynamically evolving signals remains an open question.

Studies of innate immune cells under dynamic time-varying signals proposed the existence of individual cell memory, i.e., increased or reduced signal sensitivity (priming or tolerance) due to past exposure to other signals. Cellular memory of prior stimuli may enable fine-tuned cellular decision-making by selectively amplifying and muting signals based on prior context. Thus, information processing in a complex environment can be reduced to a few key signaling features that are simpler to process by limited cellular resources. It has been suggested that retention of memory of previous signals can contextualize responses to subsequent signals during acute inflammation.[8] Macrophages are first-responder cells that sense pathogens and coordinate local and systemic immune responses.[9] Thus, macrophage memory of prior inflammatory signals may play a key role in immunity, and dysfunction in macrophage memory can lead to conditions like sepsis and chronic inflammation.[8] Understanding macrophage memory is crucial for fundamental studies and modeling of signaling and inflammation and may enable effective therapeutic approaches in infection, autoimmunity, and cancer.

Memory can shape cell responses in contradictory ways. Exposure to high concentrations of inflammatory stimuli like bacterial lipopolysaccharides (LPSs) induces tolerance and mutes

Please cite this article in press as: Wang et al., Macrophage memory emerges from coordinated transcription factor and chromatin dynamics, Cell Systems (2025), https://doi.org/10.1016/j.cels.2025.101171

subsequent response to other inflammatory stimuli.[10–12] Exposure to other classes of inflammatory stimuli or even lower concentrations of the same stimulus, however, can induce priming and amplify subsequent response to inflammatory stimuli.[13–18] These contradictory responses necessitate systematic profiling of memory encoding and identification of rules underlying cellular decisions toward priming or tolerance.[19]

Inflammatory stimuli produce global changes in chromatin accessibility and enhancer landscapes, which may contribute to cellular memory and eventually both tolerance and priming.[8,12,17] These stimuli also work at the level of signal transduction, inducing transcription of positive and negative feedback proteins in the form of signaling intermediaries, receptors, and cytokines.[15,20–23] Previous studies have not considered the multi-level regulatory nature of complex processes like memory when studying transcriptional control. In particular, cellular memory has been primarily associated with chromatin-mediated processes,[24] with less emphasis on alterations in signaling networks.

Systematic screening of dynamic signals in single cells is technically challenging and requires high throughput, time-resolved stimulation, and continuous readouts. Automated microfluidic live-cell imaging resolves these concerns by enhancing cell culture and stimulation and providing real-time readouts of cellular states. Microfluidic live-cell imaging of nuclear factor κB (NF-κB) transcription factor (TF) dynamics, in particular, has revealed key features of inflammatory signal processing over time. The NF-κB pathway is a central regulator of inflammatory signaling,[25] and temporal dynamics of NF-κB activation encode information about the identity, dose, and duration of a particular stimulus.[26–28] NF-κB dynamics in single cells are reshaped by prior stimuli and may retain the memory for prior signals.[29,30] Recently developed transgenic mouse models have shown how NF-κB dynamics play a role in primary immune cells and disease states.[28,31–33] Thus, tracking NF-κB activation dynamics in single primary immune cells is uniquely suited to characterizing the global changes in signal transduction due to memory in inflammatory signaling networks.

In this work, we profile the effects of inflammatory memory on activation dynamics of the NF-κB pro-inflammatory TFs, remodeling of chromatin accessibility, and regulation of transcriptional state. We show that the transcriptional state of memory-conditioned macrophages can be explained and predicted by changes both in cytosolic signaling dynamics and in nuclear chromatin accessibility. We use a systematic screen of 80 pairwise ligand sequences to discover that memory in primary macrophages is encoded through altering the dynamics of inflammatory signaling through NF-κB. Combining these multimodal approaches allows us to generate a deep-learning model that predicts gene expression under different memory conditions. Altogether, these results comprehensively profile and reveal how cellular decision-making can be tuned by multi-level encoding of stimulus history.

RESULTS

Sequential stimulation with inflammatory ligands results in distinct NF-κB activation dynamics in single macrophages

Leveraging the strengths of microfluidics and live-cell imaging, we systematically profiled innate immune memory in primary bone-marrow-derived macrophages generated from transgenic mice expressing a fluorescently tagged member of the canonical NF-κB family of TFs, RelA ($RelA^{v/v}$) (Figure S1A).[28,29] While prior studies of signaling memory and sequential ligand stimulus exist, our approach improves the number of testable sequences, enables single-cell resolution, and allows exploration of memory in the context of dynamic TF regulation (Figure 1A).

We began our systematic screening of signaling memory by strategic selection of six inflammatory ligands, including pro-inflammatory cytokines (tumor necrosis factor alpha [TNF-α] and interleukin [IL]-1β), bacterial molecules and analogs (CpG, PAM2CSK4 [PAM], and LPS), and viral analogs (polyI:C). Each ligand acts on one of several intracellular pathways that ultimately all converge on activation of NF-κB (Figure S1B).[34] We stimulated cells with one of these ligands (ligand A) at different doses and durations, followed by TNF-α or LPS stimulation (ligand B), producing a total of 80 dynamic inputs testing individual memory conditions (Figure S1C). TNF-α has a largely independent signaling pathway, and LPS shares many pathway intermediaries with each ligand except TNF-α, which allowed us to test the importance of shared pathway intermediaries on memory. We tracked nuclear translocation of RelA in single cells during stimulation with ligand A and ligand B, which identified clear differences in ligand B response depending on prior stimulus (Figures 1B and 1C). Distinct single-cell NF-κB activation dynamics and memory effects were visible among the 80 conditions (Figures 1E, 1F, and S2; Videos S1, S2, and S3).

For example, we considered the potential memory effect of CpG or polyI:C stimulation. CpG and polyI:C activate distinct intracellular pathways involving MyD88 and TRIF, respectively, before ultimately triggering NF-κB translocation (Figure 1D).[34] For CpG, we observed a clear attenuation of cellular response to both TNF-α and LPS, though the response to CpG increased (Figure 1E), while increased polyI:C response potentiated responses by increasing activation amplitude and durations (Figure 1F). Thus, we concluded that NF-κB dynamics encoded ligand-specific memory effects, including both attenuation, or tolerance, and potentiation, or priming.

Ligand-specific memory encodes dose- and duration-dependent tolerance and priming

Altered activation dynamics due to memory suggest that prior stimulus remodels the NF-κB signal transduction network. To quantify and compare the effects of remodeling by different stimuli, we normalized NF-κB response area-under-the-curve (AUC) from "memory-conditioned" cells to the naive AUC for the same stimulus (Figure S1D). AUC is a measure of total NF-κB activity in a given cell. Stimuli that induced a response AUC below naive were classified as tolerizing, and those that induced a response AUC above naive were considered priming. Using this quantification, we confirmed our observation that the CpG stimulus tolerized subsequent TNF-α and LPS signaling and that polyI:C stimulus primed subsequent signaling. We did not observe previously reported shifts from priming to tolerance or vice versa in our dose range, possibly due to the lack of "sub-stimulatory" doses in our screen (Figures 2A–2D). However, stimulation with increased concentrations of tolerance-inducing ligands resulted in greater attenuation of subsequent response, showing that tolerance is dose dependent. polyI:C was the only ligand to

Please cite this article in press as: Wang et al., Macrophage memory emerges from coordinated transcription factor and chromatin dynamics, Cell Systems (2025), https://doi.org/10.1016/j.cels.2025.101171

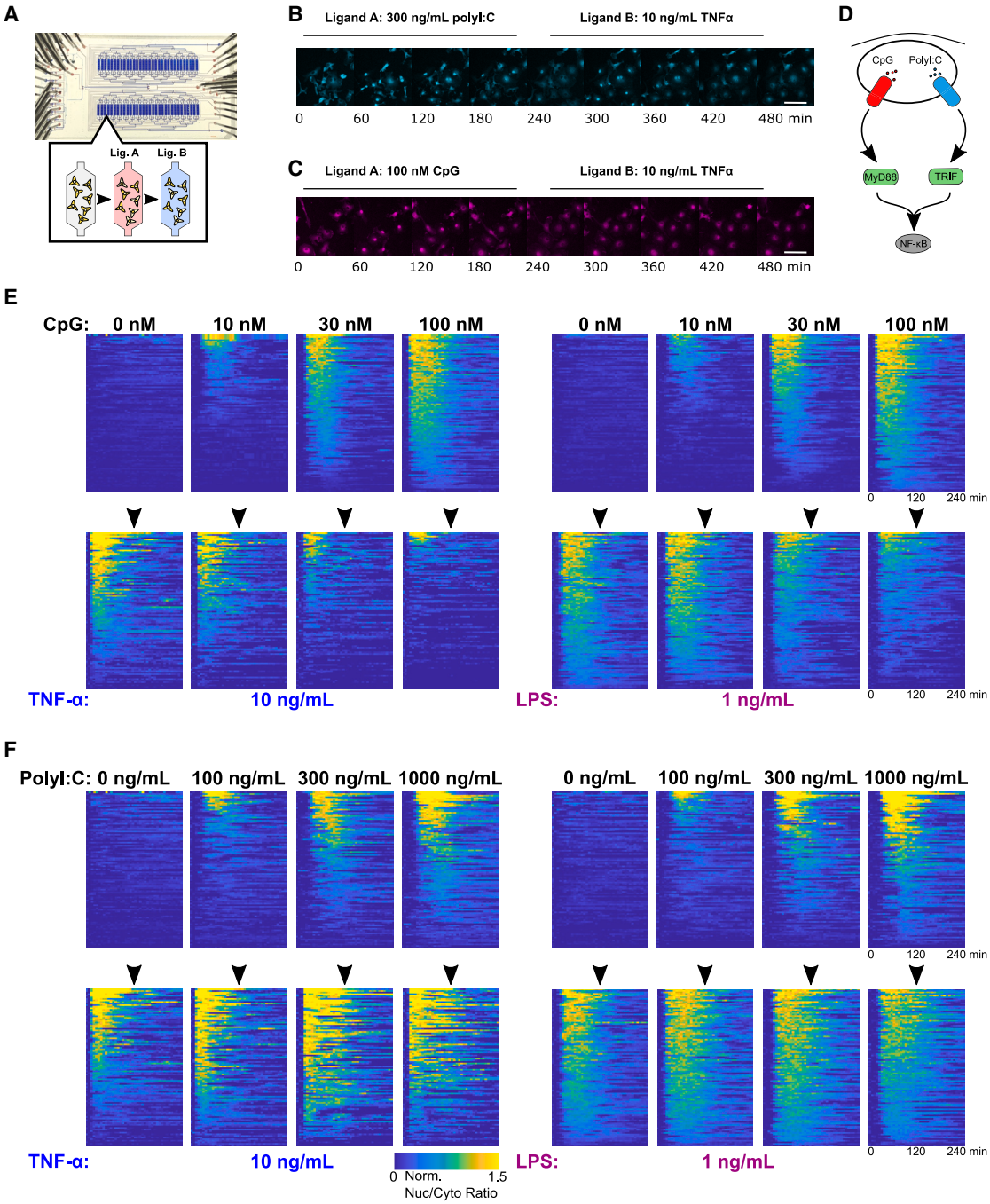

Figure 1. Microfluidic screening of memory encoded in NF-κB dynamics in single live cells

(A) Automated microfluidics enables high-throughput stimulation and continuous tracking of single cells over sequential stimuli to profile signaling memory in macrophages.

(B and C) Representative cells showing live cell imaging of primary macrophages from RelA$^{v/v}$ mice over multiple stimuli. Frames show either 300 ng/mL polyI:C to 10 ng/mL TNF-α or 100 nM CpG to 10 ng/mL TNF-α. Each condition measured over >300 individual cells. Scale bar 50 microns.

(D) CpG and PolyI:C signal transduction pathways.

(E and F) NF-κB responses to different doses of CpG (E) or PolyI:C (F) for 4 h (upper plots) followed by either TNF-α or LPS (lower plots). Single-cell tracemaps show 100 random traces sorted by the magnitude of maximum activation over 240 min of stimulation. Color indicates normalized nuclear/cytoplasmic ratio on a linear scale, with 1 being the mean amplitude at the highest dose (stimulus A) or with no prior ligand (stimulus B).

Please cite this article in press as: Wang et al., Macrophage memory emerges from coordinated transcription factor and chromatin dynamics, Cell Systems (2025), https://doi.org/10.1016/j.cels.2025.101171

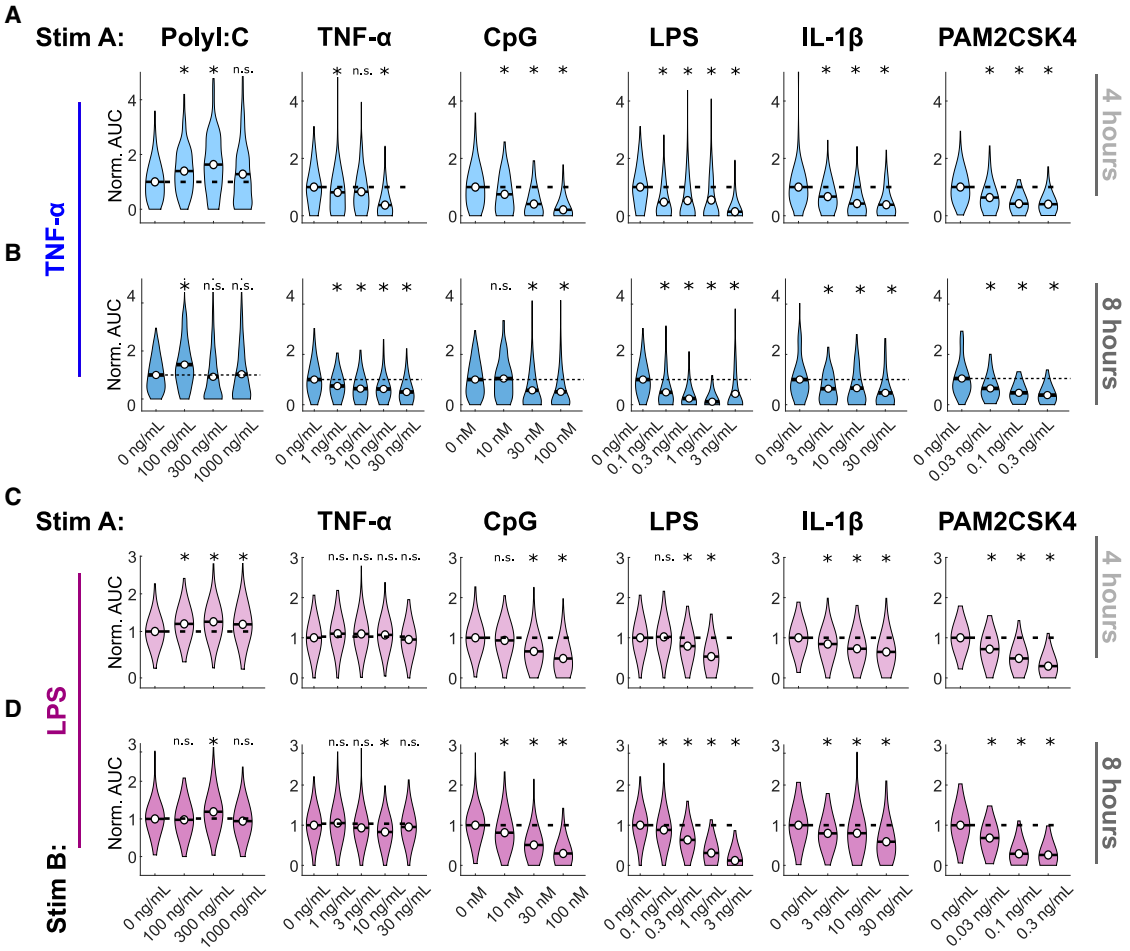

Figure 2. Stimulus identity, dose, and duration shape innate immune memory to produce both priming and tolerance

(A) Quantified normalized AUC for 10 ng/mL TNF-α response following stimulus A at the indicated dose for 4 h. Dashed black line shows AUC at baseline (normalized to 1). Open circle shows mean. $n > 100$ single cells over two independent preparations for each condition. * $p < 1 \times 10^{-2}$ by Wilcoxon rank-sum test with Bonferroni correction.

(B) Quantified normalized AUC for 10 ng/mL TNF-α response after 8 h of stimulus A. All notation is the same.

(C and D) Quantified normalized AUC for 1 ng/mL LPS response after 4 (C) or 8 (D) h of stimulus A. All notation is the same as in (A).

produce priming and showed weak to no dose dependency (Figures 2A and 2C).

Generally, memory in macrophages affected subsequent TNF-α and LPS stimulus similarly, unlike previous reports that memory in NF-κB dynamics is dependent on overlap between stimulus pathways in fibroblasts.[30,35] TNF-α, however, tolerized only subsequent TNF-α re-stimulus, which may be due to pathway-specific negative feedback (Figures 2A and 2B).[36] Increasing stimulus duration resulted in a greater magnitude of tolerance, especially at higher doses (Figures 2B and 2D). However, PolyI:C priming weakened with longer stimulus duration, suggesting that maximal PolyI:C priming may take place within the first 8 h and wane over time (Figure 2B). Our initial screen thus identifies ligand-specific priming and tolerance in a dose- and duration-dependent manner.

To understand whether priming and tolerance are encoded and can be classified on a single-cell level, we measured the mutual information between different memory-conditioned responses. Mutual information can be used to quantify the accuracy of signal transduction.[26,28,30] In this context, mutual information between two conditions with the same stimulus but different prior stimuli indicates the accuracy with which stimulus response dynamics reflect a cell's memory state.

Broadly speaking, NF-κB dynamics in single cells can highly distinguish between prior stimuli. Comparing TNF-α response after either 4 or 8 h of prior stimulus revealed up to 0.9 bits of mutual information, which represents near-complete distinguishability (Figures 3A and 3B). In particular, the TNF-α response after polyI:C treatment was highly distinguishable from naive and other prior stimuli, consistent with polyI:C being uniquely priming. Other stimuli like IL-1β are largely indistinguishable from all other memory conditions, perhaps reflecting a high intercellular variability in the memory response following IL-1β. Similarly, LPS response produced variable mutual information based on prior stimulus (Figures 3C and 3D). PolyI:C treatment did not result in notably greater mutual information

Please cite this article in press as: Wang et al., Macrophage memory emerges from coordinated transcription factor and chromatin dynamics, Cell Systems (2025), https://doi.org/10.1016/j.cels.2025.101171

CellPress

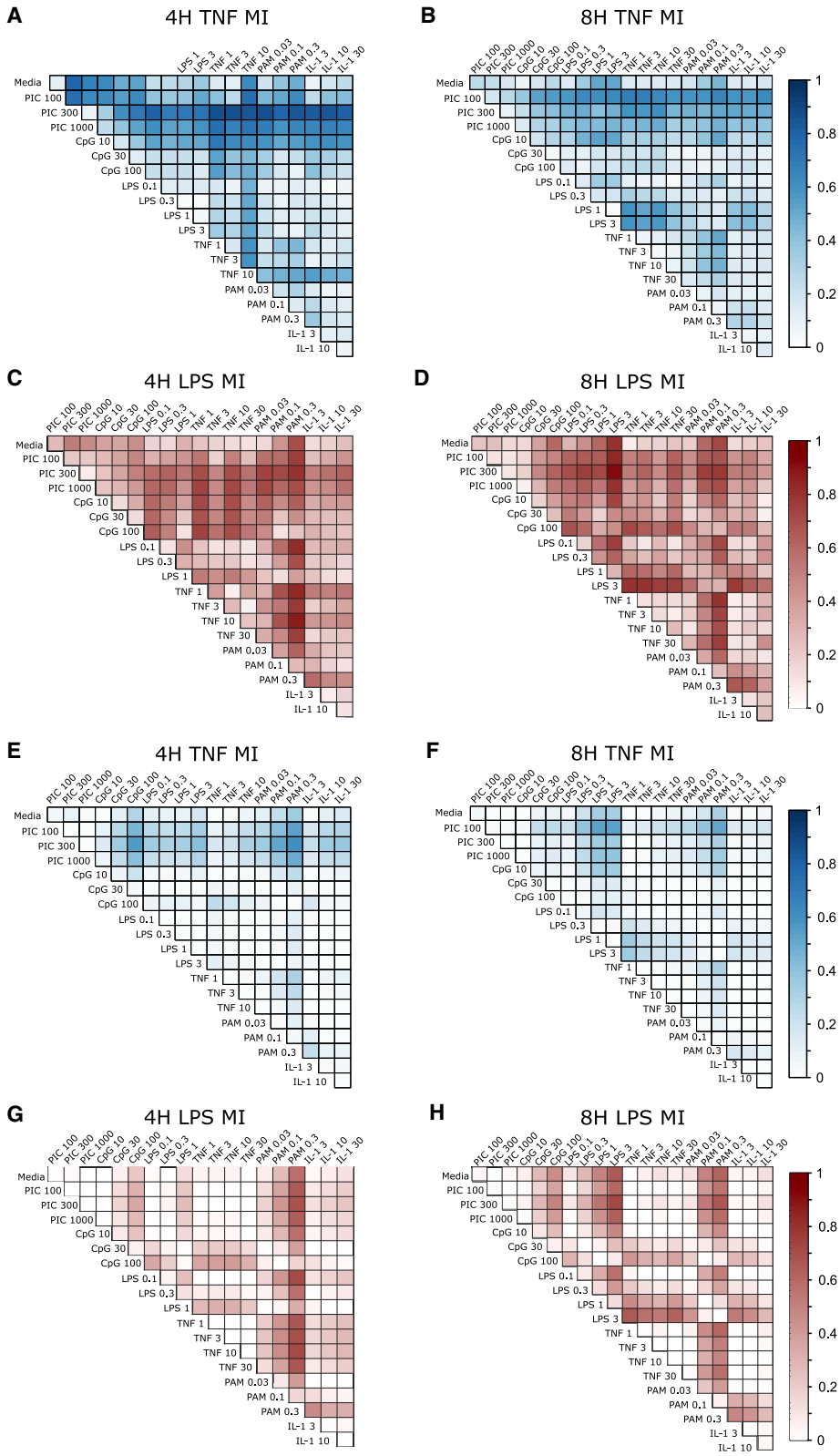

(legend on next page)

Please cite this article in press as: Wang et al., Macrophage memory emerges from coordinated transcription factor and chromatin dynamics, Cell Systems (2025), https://doi.org/10.1016/j.cels.2025.101171

for the LPS response, perhaps due to the weak priming effect on polyI:C on the LPS response. Instead, the highest doses of LPS and PAM were strongly distinguished from nearly every other condition, reflecting the strongly tolerogenic nature of these stimuli. Taken together, these results show that distinct memory states can produce highly distinguishable NF-κB response dynamics to identical stimuli.

Mutual information can also be calculated using a single feature of the NF-κB response, which allows us to compare the information transferred by a dynamic process versus a key metric. We used maximum response amplitude as a proxy for response magnitude in each condition and repeated the same comparisons (Figures 3E–3H). Mutual information based on a maximum amplitude was significantly lower than that from the entire trace. The only conditions that remained largely distinguishable were LPS following the highest doses of PAM or LPS, which is consistent with strong tolerance being well reflected in response magnitude (Figures 3G and 3H). Thus, NF-κB response dynamics convey essential information about stimulus memory in single cells, which is lost by reducing the dynamic response to a single feature.

NF-κB dynamics encode memory of *in vivo* inflammatory challenge in peritoneal macrophages

After observing that signaling memory alters NF-κB activation dynamics in bone-marrow-derived macrophages, we asked whether acute inflammation *in vivo* also induces similar memory effects in tissue macrophages. Murine endotoxin tolerance is a classic model of innate immune memory where sublethal endotoxemia protects against lethal rechallenge,[10] and the role of macrophage memory in this phenomenon has been well described in previous studies.[11,12,37] In particular, immunosuppression induced by sepsis is a clinically important phenomenon related to this memory effect.[38] We hypothesized that endotoxin challenge encodes signaling network-level changes that manifest as altered signaling dynamics to rechallenge.

We used a mouse model of sublethal endotoxemia via peritoneal injection of LPS (Figure S3A), followed by isolation and microfluidic culture of primary peritoneal macrophages from endotoxemic and sham-injected mice (Figures 4A and S3B–S3D). Peritoneal macrophages cultured without stimulus showed minimal activation and good adaptability to microfluidic culture (Figures 4B and 4E). Treatment with TNF-α and LPS revealed clear differences in NF-κB activation dynamics. While nearly all macrophages from saline-treated mice activated following stimulation, response to TNF-α is significantly attenuated, and response to LPS is completely abolished in macrophages from endotoxin-treated mice (Figures 4C–4E). Endotoxemia also significantly delayed and increased the heterogeneity in the time to activation following treatment with TNF-α and LPS (Figure 4F) and reduced the amplitude of activation (Figure 4G). We concluded that innate immune memory phenotypes like endotoxin tolerance can indeed be encoded by adult macrophages in the form of altered NF-κB dynamics.

Unlike in bone-marrow-derived macrophages, TNF-α activation dynamics in peritoneal macrophages showed an extended activation plateau instead of an activation pulse (Figure 4C). Endotoxemia attenuated LPS-induced dynamics more strongly than TNF-α-induced dynamics (Figures 4C and 4D), while TNF-α was generally more attenuated than LPS in bone-marrow-derived macrophages (Figure 2). These results suggest important differences in how inflammatory stimuli are sensed and converted into NF-κB dynamics in different innate immune contexts.

Chromatin accessibility dynamics regulate TF targets following macrophage activation

Having shown that inflammatory memory is mediated through reshaping the dynamics of NF-κB signaling, we then turned to how memory changes the intranuclear targets of activated inflammatory TFs. Chromatin accessibility rapidly changes after exposure to inflammatory stimulus,[39] and remodeling of promoters and enhancers has been shown to tune the transcriptional response to subsequent stimuli over days to weeks. We hypothesized that even on the timescale of hours, inflammatory memory is the product of both modulation of TF dynamics and chromatin accessibility, which changes the nuclear targets of that TF (Figure 5A). We performed ATAC-seq to profile accessible chromatin for single and sequential stimulus conditions to test this possibility.

We observed that CpG and polyI:C treatment produced distinct changes in chromatin accessibility (Figure 5B; Table S1). Hierarchical clustering identified regions with increased accessibility after both polyI:C treatment and CpG treatment, as well as only after each individually, indicating stimulus-dependent opening of chromatin. Interestingly, all three upregulated groups showed enrichment for κB and activated protein 1 (AP-1) motifs, which are the predominantly activated TFs downstream of Toll-like receptor (TLR) signaling (Figure 5B; Table S2). The polyI:C-specific and shared groups were also enriched for interferon-stimulated regulatory elements (ISREs), while the CpG-specific group was enriched for CCAAT/enhancer binding protein (c/EBP) motifs. Thus, these observations correspond with activation of NF-κB, c-Jun N-terminal kinase (JNK), and p38 signaling by both polyI:C and CpG, while only polyI:C induces an interferon program, as is consistent with the literature.[40] c/EBP activation by CpG has not been described, but the c/EBP family of TFs coordinates initial responses to inflammatory stimuli and controls myeloid differentiation and could be a target of TLR9 activation.[41]

We saw enrichment of RelA motifs in regions of polyI:C-specific, CpG-specific, and shared increased peak accessibility (Figure 5B). We asked whether regulation of RelA sites by neighboring TFs could explain the different regulatory modes for one TF motif. Indeed, polyI:C upregulated RelA peaks strongly

Figure 3. Response dynamics to identical stimulus are distinguished by memory of prior stimulus using informational theory

(A–D) Mutual information (MI) calculated from dynamic vector of 20 evenly spaced time points over the 4 h stimulus interval. All conditions compared within one heatmap are the same stimulus after 4 (A and C) or 8 (B and D) h of ligand A. Ligand A dose ordered from lowest (1) to highest (3 or 4). MI shown in bits, where 1 indicates full distinguishability and 0 indicates indistinguishability.

(E–H) Same MI calculations but from a single feature (maximum amplitude) instead of a dynamic vector.

Please cite this article in press as: Wang et al., Macrophage memory emerges from coordinated transcription factor and chromatin dynamics, Cell Systems (2025), https://doi.org/10.1016/j.cels.2025.101171

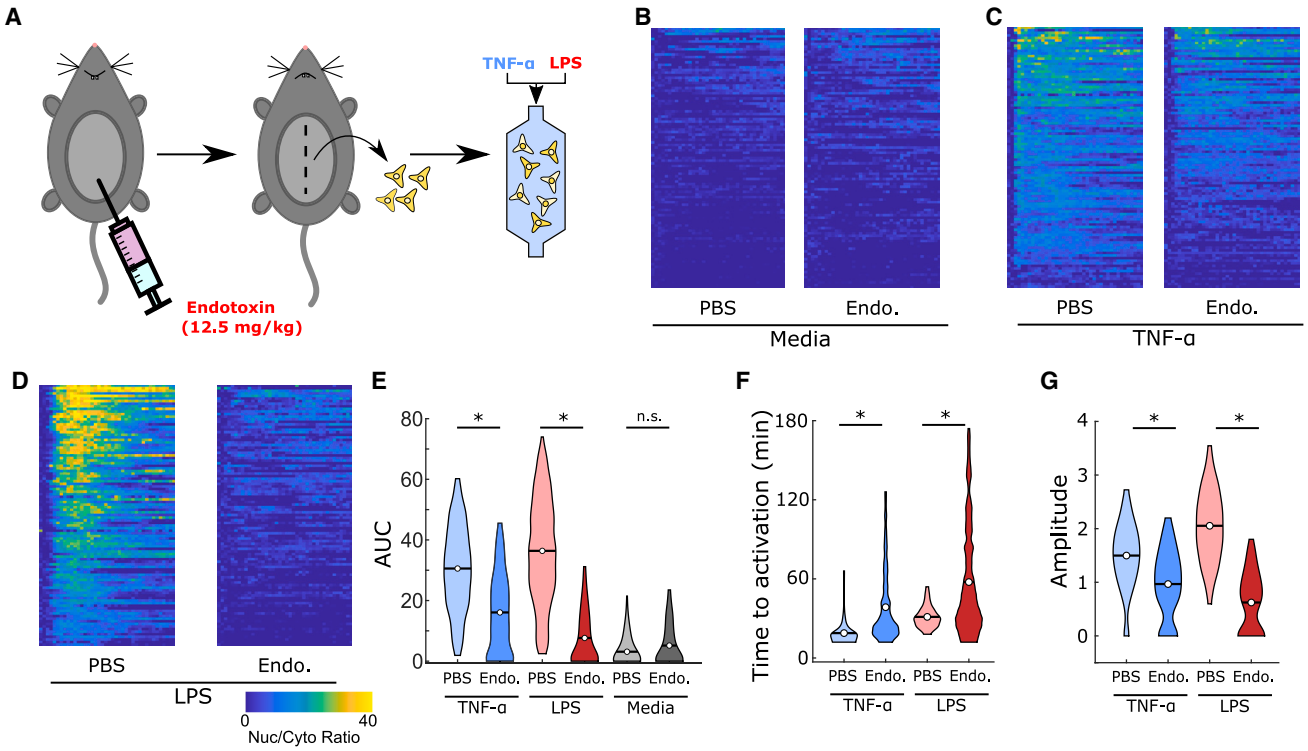

Figure 4. *In vivo* endotoxin tolerance is encoded in adult macrophages through changing NF-κB dynamics

(A) Schematic for endotoxemia and adult macrophage retrieval.

(B–D) NF-κB dynamics in adult peritoneal macrophages from mice injected with PBS or endotoxin. 100 random traces selected from >200 cells (B) or >600 cells (C and D) over 3 mice/condition.

(B) Baseline NF-κB dynamics.

(C) NF-κB dynamics following 10 ng/mL TNF-α.

(D) NF-κB dynamics following 1 ng/mL LPS.

(E–G) Violin plot of total AUC (E), time to activation (F), or activation amplitude (G) over 4 h for each condition. Open circle shows mean. *p value < 0.01, n.s. p value > 0.01 by Wilcoxon ranked sum test with Bonferroni correction.

co-occur with ISREs (Figure 5C). Likewise, CpG-upregulated RelA peaks co-occur with c/EBP motifs. The co-occurrence of AP-1 motifs with RelA is quite similar across all groups (Figure 5C). These suggest that stimulus-specific tuning of epigenetic accessibility at RelA binding sites may be due to interactions between these binding sites and neighboring, stimulus-specific TFs and binding sites.

We also asked whether stimulus-induced changes in chromatin accessibility can be overwritten by subsequent stimuli. We profiled chromatin accessibility following sequential stimuli with polyI:C/CpG to TNF-α/LPS (Table S1) and identified differentially accessible regions (Figures S4A and S4B). Despite the subsequent TNF-α/LPS stimulus, differentially accessible regions still primarily grouped based on the first polyI:C and CpG stimulus and were enriched for similar motifs (Figure S4C; Table S2). Since it appeared that the first stimulus played an outsized role in determining which regions exhibited differential accessibility, we asked whether the chromatin landscape in sequentially stimulated samples more resembled the chromatin landscape induced by the first stimulus alone (polyI:C/CpG) or the second stimulus alone (TNF-α/LPS) (Figures 5D and 5E). Correlation between sequential stimuli and the landscape induced by the first polyI:C/CpG stimulus was generally much stronger than correlation with the second stimulus landscape. We concluded that initial stimulus exposure plays a lasting role in determining the chromatin accessibility landscape for a cell and is difficult to overwrite by subsequent stimuli.

Overall, these results show that stimulus-induced chromatin accessibility changes take place on the timescale of hours. We identify stimulus-specific TF motifs that may cooperatively tune chromatin accessibility. Finally, we show that initial inflammatory exposure produces lasting effects that persist even after re-exposure with another stimulus.

Memory-induced TF and chromatin accessibility dynamics are encoded into cellular decision-making

Having identified mechanisms of inflammatory memory encoding in both TF activation and chromatin accessibility dynamics, we finally turned to whether this memory was encoded in the macrophage transcriptional program. We performed RNA sequencing for four representative cases, polyI:C or CpG to TNF-α or LPS, which include both priming and tolerance based on NF-κB dynamics and distinct chromatin accessibility signatures based on ATAC sequencing. Transcripts were classified by whether they were synergistically or antagonistically regulated by prior stimulus (Figure 6A; Table S3). Synergistic

Please cite this article in press as: Wang et al., Macrophage memory emerges from coordinated transcription factor and chromatin dynamics, Cell Systems (2025), https://doi.org/10.1016/j.cels.2025.101171

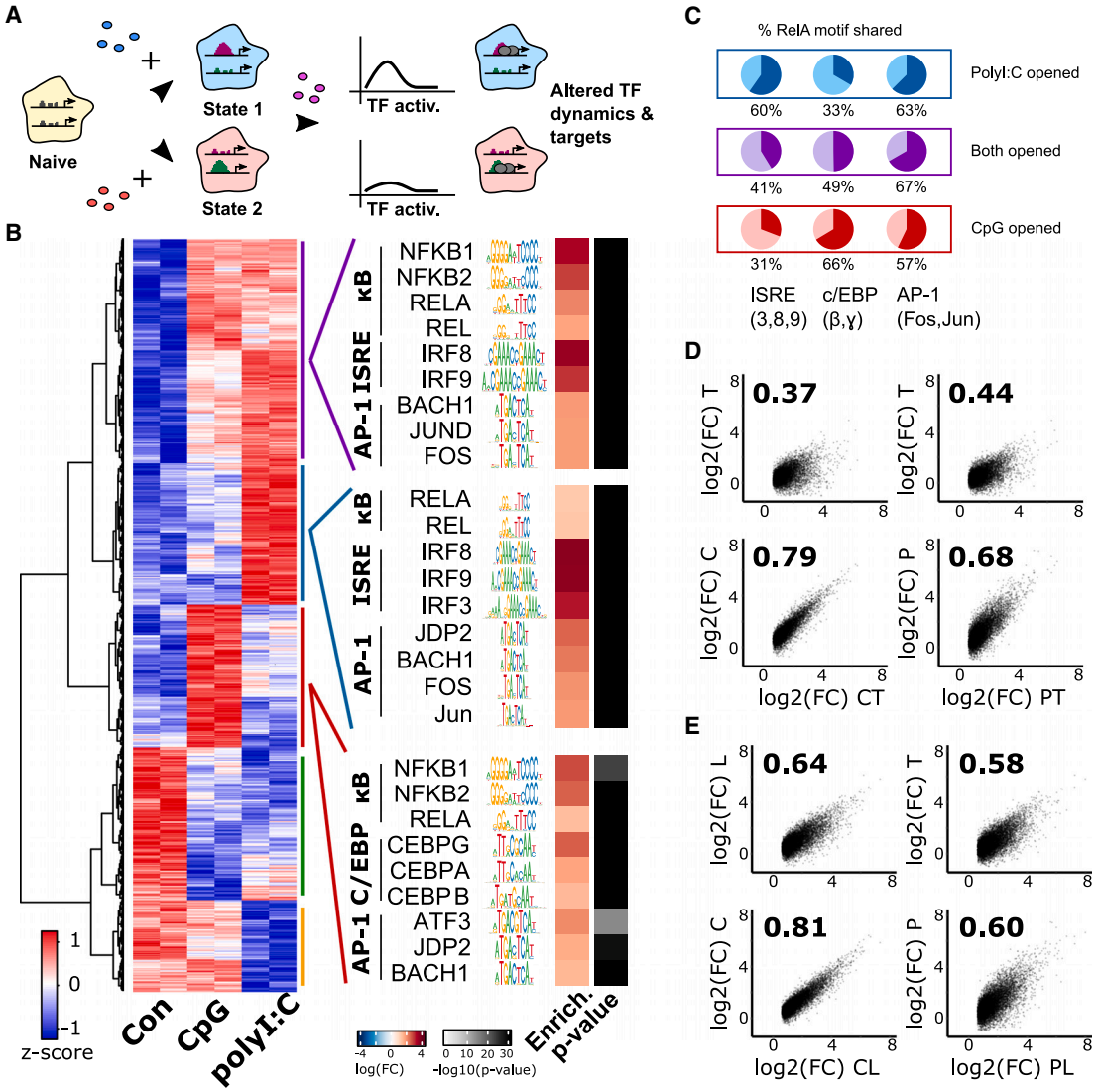

Figure 5. Chromatin accessibility is associated with tolerance- and priming-specific memory effects in macrophages

(A) Model of how memory mediates changes in both transcription factor dynamics and targets through chromatin accessibility dynamics.

(B) Heatmap of differential accessibility following CpG or polyI:C stimulus. Groups clustered using the Ward algorithm. A subset of enriched motifs for each group is shown on the side. Colors linearly scaled.

(C) Fraction of differentially open RelA peaks (MA0107.1) that share Irf3, 8, and 9 motifs (MA0652.1, MA0653.1, and MA1418.1), c/EBP β and γ motifs (MA0838.1 and MA0466.1), or Fos and Jun motifs (MA0476.1 and MA0488.1).

(D) Scatterplots comparing fold-change in accessibility for upregulated regions after 4 h of CpG or polyI:C and 4 h of TNF-α to the same regions following 4 h of CpG or polyI:C only or 4 h of TNF-α only. Spearman correlation coefficient for each comparison shown above.

(E) Same as (D), except following 4 h of CpG or polyI:C and 4 h of LPS compared with 4 h of CpG or polyI:C only or 4 h of LPS only.

regulation implies that memory of prior stimulus induces transcription beyond the independent contributions of each stimulus, while antagonistic regulation implies that memory induces less transcription than the independent contributions of each stimulus (STAR Methods).

Since NF-κB activation is strengthened following priming and weakened following tolerance, we expected more antagonistic genes due to tolerance and more synergistic genes due to priming. Consistent with our expectations, we only identified 214 synergistically regulated transcripts and 366 antagonistically regulated transcripts for CpG to TNF-α stimulus, compared with 572 synergistic and 394 antagonistic transcripts for polyI:C to TNF-α (Figures 6B and 6C). We repeated this analysis for polyI:C/CpG to LPS and found that polyI:C and CpG induced similar numbers of synergistic transcripts but that CpG stimulus produced 30% more antagonistic transcripts (Figures S5A and S5B). To identify cellular processes associated with synergy and antagonism, we performed overrepresentation analysis on selected transcripts. Synergistic transcripts from all conditions were enriched for immune and inflammatory responses, while those due to priming were also enriched for NF-κB and TNF signaling (Figure 6D; Table S4). Similarly, antagonistic transcripts

Please cite this article in press as: Wang et al., Macrophage memory emerges from coordinated transcription factor and chromatin dynamics, Cell Systems (2025), https://doi.org/10.1016/j.cels.2025.101171

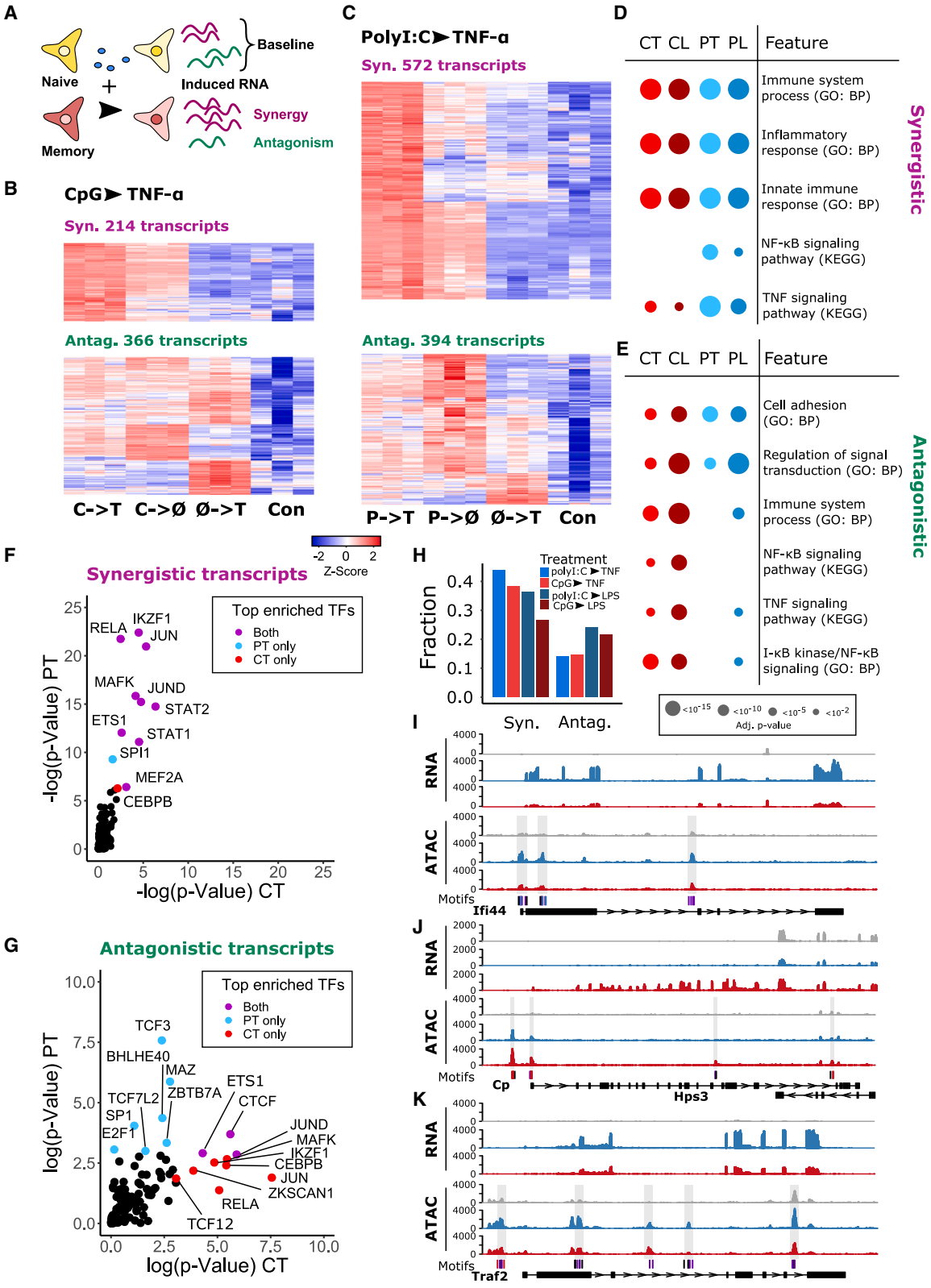

Figure 6. Gene expression profiling reveals distinct transcriptomic changes due to tolerance or priming

(A) Approach for determining memory-based synergy and antagonism in gene expression.

(B) Heatmaps of synergistically or antagonistically upregulated genes for CpG to TNF-α. RNA-seq was performed in triplicate, and each row is one gene.

(legend continued on next page)

Please cite this article in press as: Wang et al., Macrophage memory emerges from coordinated transcription factor and chromatin dynamics, Cell Systems (2025), https://doi.org/10.1016/j.cels.2025.101171

from all conditions were enriched for cell adhesion and signal transduction, but those associated with tolerance were more enriched for NF-κB and TNF signaling (Figure 6E; Table S4). Taken together, these results suggest that while memory globally increases transcription of a subset of genes associated with inflammatory signaling, genes specific to NF-κB and TNF signaling are synergistically regulated by priming but antagonistically regulated by tolerance.

Since we observed increased chromatin accessibility at distinct sites following stimulus, we hypothesized that chromatin accessibility accounted for a subset of transcriptional outcomes in synergy and antagonism as well. Namely, NF-κB and AP-1 should be involved in regulating both polyI:C- and CpG-induced memory, while signal transducer and activator of transcription (STAT) and interferon regulatory factors (IRFs) should regulate polyI:C-induced memory, and c/EBP TFs should regulate CpG-induced memory. We used the ChEA3 algorithm to identify TFs predicted to be associated with synergistic and antagonistic transcriptional regulation based on published ENCODE chromatin immunoprecipitation sequencing (ChIP-seq) data.[42] Synergistic transcripts for both polyI:C and CpG stimulus shared a large fraction of enriched TFs, including the expected NF-κB (RelA) and AP-1 (Jun and JunD) family TFs, but also interferon-related TFs (Stat1 and Stat2) (Figure 6F). These TFs were generally more enriched following polyI:C priming, consistent with the more synergistic regulation of transcription with priming. By contrast, antagonistic transcripts largely did not share enriched TFs, with CpG-specific TFs including many of those involved in NF-κB and JNK signaling (Figure 6G). Additionally, Cebpb, a c/EBP TF, was indeed overrepresented for CpG-induced synergy and antagonism. These results suggest that CpG-induced synergy and antagonism in different subsets of genes regulated by the same TFs. Applying the same overrepresentation analysis to the polyI:C or CpG to LPS conditions also showed shared TFs among the synergistic genes and more distinct TFs among antagonistic transcripts (Figures S5C and S5D).

We then tested our hypothesis that synergistic gene expression is associated with increased accessibility at chromatin sites in the promoter region for these genes. We identified genes with upregulated promoter and proximal enhancer peaks (± 3,000 bp from the transcriptional start site) following polyI:C or CpG stimulus and found that genes synergistically regulated by memory were more likely to have increased promoter accessibility following both polyI:C and CpG stimulus (Figure 6H). Thus, chromatin accessibility contributes to regulating synergy and antagonism in transcription.

From our ATAC findings, we identified TF motif "signatures" that co-occurred in sites of increased accessibility following polyI:C priming (NF-κB, AP-1, and ISRE) and CpG tolerance (NF-κB, AP-1, and c/EBP). Using transcriptional data, we found that the co-occurrence of these motifs also corresponds to synergistic regulation of gene expression. For example, *Ifi44* primarily contains RelA and ISRE motifs in the promoter region and is synergistic for polyI:C to TNF-α stimulation (Figure 6I). *Cp* contains RelA and c/EBP motifs and is synergistic for CpG to TNF-α (Figure 6J). *Traf2* is synergistic for both conditions and contains RelA and AP-1 motifs (Figure 6K). Interestingly, the TF signature for CpG tolerance was overrepresented in both synergistic and antagonistic transcriptional regulation (Figures 6F and 6G), which suggests that this set of TFs may be associated with both up- and downregulation of target genes. To profile which expression programs are turned on and off by tolerance, we looked at cellular processes associated with the 96 synergistic and 325 antagonistic transcripts regulated by at least one of these seven shared TFs. We found that synergistic transcripts were enriched for IFN-γ signaling and proliferation, while antagonistic transcripts were enriched for metabolism, NF-κB signaling, and mitogen-activated protein kinase (MAPK) signaling (Figure S6E). Although IFN-γ is not expressed by our BMDMs, the IFN-γ GO term may reflect Stat1/2 activation by type I interferons (Figure 5B; Table S4). Thus, memory may "fine-tune" TF activity to synergize particular gene programs and antagonize others.

Coordinated TF dynamics and chromatin accessibility enable signaling memory and gene expression control

Based on our observations that memory-dependent changes in both TF dynamics and chromatin accessibility corresponded to synergistic and antagonistic gene regulation, we hypothesized that combining chromatin and NF-κB dynamics features could predict transcriptional regulation. We trained a convolutional neural network that integrated 133 chromatin accessibility features, including peak accessibility and associated motifs, and 48 features of TF dynamics, to classify gene expression into downregulated, unchanged, upregulated, and highly upregulated bins in response to any one of 8 stimulus conditions (Figures 7A and S6). This classification challenge is not trivial, as most deep learning approaches to predicting gene expression are only able to classify cell-type-specific gene expression signatures from chromatin signatures at steady state.[43,44] Here, we seek to predict perturbation-specific gene expression changes in a single-cell type based on changes in accessibility and activity. Our resultant multilayer perceptron model classifies gene expression with 72.8% accuracy, an improvement of over 30% from random assignment (Figures 7B and 7C). Importantly, our model predicts stimulus-dependent changes in gene

(C) Same as (B) for polyI:C to TNF-α. Colors linearly scaled in both heatmaps.
(D and E) *p* values from overrepresentation analysis of synergistic (D) or antagonistic (E) genes for the indicated treatment conditions. Gene sets from either GO: BP or KEGG databases. Size of circle corresponds to adjusted *p* value.
(F) Scatterplot of overrepresented TFs from synergistically regulated genes following either CpG to TNF-α (CT) or polyI:C to TNF-α (PT). Top 10 TFs for each condition colored based on whether they are overrepresented for PT (blue), CT (red), or both PT and CT (purple). Enrichment *p* values based on ChEA3 using the ENCODE TF target library.
(G) Same as (F) for antagonistically regulated genes following either CT or PT.
(H) Barplot showing fraction of synergistic or antagonistic transcripts for each treatment condition with increased promoter accessibility following polyI:C or CpG treatment.
(I–K) Tracks from RNA-seq (media, gray; P→T, blue; and C→T, red) and ATAC-seq (media, gray; polyI:C, blue; and CpG, red) for synergistic genes in P→T (I), C→T (J), or both (K). RelA motifs (black), Irf3 and Irf8 motifs (blue), c/EBPγ motifs (red), and Fos motifs (purple) shown below tracks. Called peaks shaded in gray.

Please cite this article in press as: Wang et al., Macrophage memory emerges from coordinated transcription factor and chromatin dynamics, Cell Systems (2025), https://doi.org/10.1016/j.cels.2025.101171

CellPress

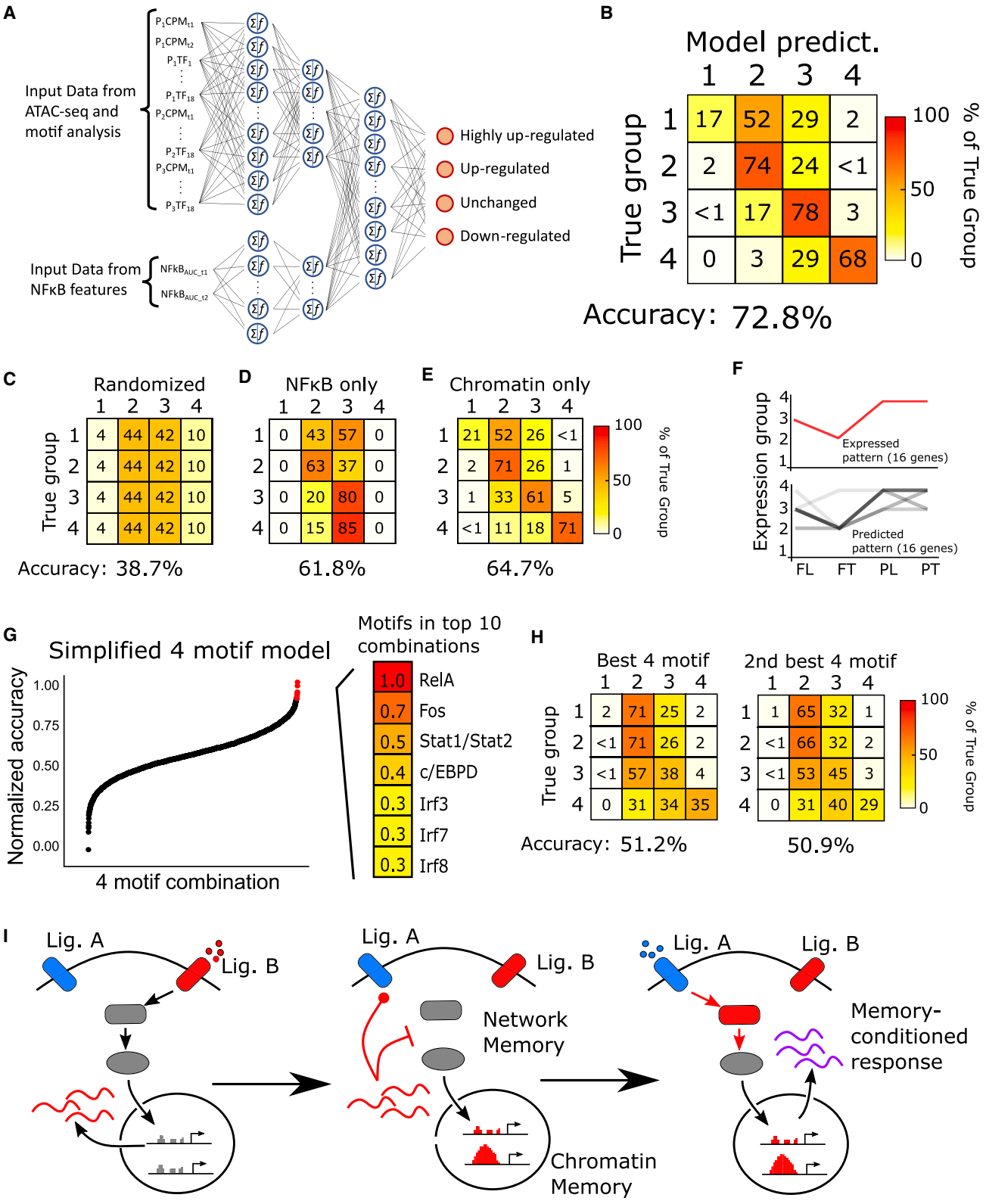

Figure 7. Deep learning based on dynamic variation in chromatin accessibility and transcription factor activation predicts transcriptional regulation

(A) Structure for neural network used to predict gene expression.

(legend continued on next page)

Please cite this article in press as: Wang et al., Macrophage memory emerges from coordinated transcription factor and chromatin dynamics, Cell Systems (2025), https://doi.org/10.1016/j.cels.2025.101171

expression. We identified 16 genes that displayed the same regulatory pattern following stimulation with LPS, TNF-α, and LPS or TNF-α after polyI:C. Despite the variability in transcriptional regulation depending on stimulus, the majority of these 16 genes were successfully predicted by our model (Figure 7F). Thus, information from dynamic changes in chromatin accessibility and TF activity was sufficient to identify characteristics of memory-based gene regulation.

We noticed that both the chromatin accessibility and TF activation data were necessary for the most accurate prediction of gene expression. A model using only NF-κB activation data classified gene expression with only 61.8% accuracy, doing particularly well at predicting upregulated genes (group 3), but entirely failing to predict downregulated (group 1) or highly upregulated (group 4) genes (Figure 7D). By contrast, the chromatin accessibility-based model was comparably more effective at predicting groups 1 and 4 while less effective at distinguishing group 3, with an overall accuracy of 64.7% (Figure 7E). Thus, both TF activation dynamics and chromatin state provide necessary information for the classification of memory-induced transcriptional control.

We then sought to simplify the model and identify the features that were most important for accurate gene expression prediction. In particular, we sought to narrow the list of 18 TF motifs down to 4 motifs that were most important for predicting gene expression as a way of understanding key TFs in the gene regulatory network. Motifs that are more important for accurate prediction are more likely to be involved in biological regulation of gene expression in inflammation and inflammatory memory. RelA was enriched in all the most accurate motif combinations, consistent with our observation of RelA signaling dynamics and motif involvement in chromatin reorganization and transcription (Figure 7G). In addition, ISREs (STAT1::STAT2, IRF3, IRF7, and IRF9), AP-1 motifs (Fos), and c/EBP motifs (c/EBPD) were all highly represented in motifs with high predictive accuracy, suggesting that these motifs are important for regulation of transcription. The accuracy of prediction using only this subset of chromatin accessibility and TF motif data was reduced compared with the full chromatin model at only around 51% accuracy for the best motifs (Figure 7H) but still was significantly greater than random assignment. This finding demonstrated that these motifs both exhibit dynamic regulation under evolving inflammatory stimuli and are important mediators of gene expression themselves. Altogether, our deep-learning model showed that a combination of TF dynamics and chromatin accessibility features are necessary and sufficient to predict gene regulation with high accuracy.

DISCUSSION

In this work, we study the role of two distinct molecular mechanisms that combine to create transcriptional memory in macrophages: reprogramming of the NF-κB signal transduction network and remodeling of chromatin architecture. We discover that these mechanisms synergize to create and regulate transcriptional responses to future challenges based on memory of past exposure. Systematically profiling the effect of ligand identity, dose, and duration on memory in individual primary macrophages, we show that both priming and tolerance can be encoded in NF-κB activation dynamics. By building a deep-learning model based on measured NF-κB dynamics and memory-induced changes in gene expression, we successfully predict transcriptional responses to different stimulus patterns and show that both facets of memory encoding are vital for gene expression (Figure 7I).

We describe NF-κB dynamics in primary peritoneal macrophages, adding to a limited literature on inflammatory signaling dynamics in adult primary cells.[28,32,33,45] Interestingly, we find distinct differences between both the patterns of dynamics in peritoneal macrophages compared with BMDMs and in the way memory affects TNF-α and LPS signaling in each cell type. These differences are suggestive of fundamental differences in how signal transduction takes place in these cell types, despite their apparent similarity. In addition, the complex physiological context of endotoxemia may shape memory differently from *in vitro* stimulation due to cell-cell interactions and other factors. Further investigation into signaling dynamics in different cell types and contexts would likely reveal heretofore unappreciated subtleties in how cell types and contexts tune inflammatory signaling.

By identifying the contribution of altered NF-κB dynamics to memory, we show that remodeling of signaling networks can play a role in both tolerance and priming. Unlike adaptive immune memory, which is encoded in genomic variability and DNA-level changes, it is well established that changes in the epigenetic landscape, whether through histone modification or chromatin accessibility, encode innate immune memory through altering TF targets in the nucleus.[8,11,12] However, we demonstrate that, upstream of TF binding, TF activation dynamics can be rendered inactive or enhanced based on priming and tolerance by prior stimulus. In particular, priming,

(B) Heatmap of model prediction accuracy for gene expression in each of four classes of regulation. Overall accuracy across all genes provided below. 1 corresponds to downregulated, 2 corresponds to unchanged, 3 corresponds to upregulated, and 4 corresponds to highly upregulated.
(C–E) Heatmap of model prediction for variations of our optimal neural network.
(C) Random assignment without prediction.
(D) Prediction using only NFκB translocation features.
(E) Prediction using only chromatin accessibility and motif features.
(F) True and predicted expression patterns for 16 representative genes with variable regulation depending on condition. 11/16 genes are perfectly predicted across 4 conditions, with all genes being correctly predicted in at least 2 conditions.
(G) Quantification of the most important TF motifs for predicting gene expression. Out of 3,028 different combinations of 4 motifs, the top 10 most accurate motif predictors are enriched for RelA, Stat1/Stat2, Irf1, Jun, Fos, and c/EBPD motifs.
(H) Heatmap of model prediction using only ATAC features associated with the best (RelA, Fos, Irf7, and Irf8) and second-best (RelA, Fos, c/EBPD, and Stat1/Stat2) 4 motif combinations. Colors linearly scaled in all heatmaps.
(I) Summary model: feedback-encoded memory in the signaling network and chromatin-encoded memory combine to produce transcriptional outcomes.

which was previously thought to take place entirely epigenetically, also acts through enhancing signaling dynamics.[24] Our predictive model demonstrates that the information encoded in altered NF-κB dynamics is crucial for predicting the cell's transcriptional response. It is striking that the dynamics of a single TF can play such a role in informing transcriptional behavior, and including the dynamics of other key TFs such as the IRFs, STATs, and c/EBPs will likely further contextualize transcriptional decisions. Network-level targeting to modify signaling dynamics presents a possible avenue for therapeutic modulation of innate immune memory in pathologic states.

Innate immune memory on the timescale of hours is physiologically critical due to rapid cytokine changes in acute inflammation and the early role of the innate immune response in inflammatory response.[46,47] However, memory has primarily been studied over days to months. We show, in a mouse model of sublethal endotoxemia, that peritoneal macrophages undergo extremely rapid changes in cell state, rendering them entirely tolerant to LPS re-stimulus after only 4 h of endotoxemia. Further study of innate immune memory in the early response to acute inflammation and infection will likely reveal further adaptation and memory at this timescale.

Our work demonstrates comprehensively that signaling memory is mediated by both network and chromatin remodeling and can be deterministic in single cells but has been largely conducted in an *in vitro* model of inflammatory signaling. We show the *in vivo* relevance of network remodeling and altered signaling dynamics in a model of murine endotoxemia, but further study of macrophage signaling memory under acute and chronic inflammatory stimuli is warranted. This work would link macrophage signaling dynamics and memory to highly relevant disease states.

Profiling of signaling dynamics through multiple pathways may also provide increased insight for signaling memory from inflammatory stimulus. While there is a large body of work on dynamics in the NF-κB pathway and their relevance for inflammatory signaling, we propose a broader model where network remodeling at the level of signaling pathways adjusts the flux of signal passing into the nucleus. This process likely takes place in other contexts like the MAPK and interferon pathways as well and is worthy of study.

RESOURCE AVAILABILITY

Lead contact

Further questions and requests for reagents and resources should be directed to the lead contact, Savaş Tay (tays@uchicago.edu).

Materials availability

This study did not generate new, unique materials.

Data and code availability

- Raw high-throughput sequencing data have been submitted to the GEO repository and are available at GSE260996 (RNA) and GSE261647 (ATAC). Single-cell NF-κB trace data reported in this paper are available at Zenodo: https://doi.org/10.5281/zenodo.14337874.
- Code is uploaded to GitHub and accessible at https://github.com/tay-lab/macrophage_memory. The DOI is listed in the key resources table.
- Any additional information required to reanalyze the data reported in this paper is available from the lead contact upon request.

ACKNOWLEDGMENTS

The authors thank Tay Lab members for reading and advising on the paper. This work is supported by NIH grants R01GM128042, R01GM127527, R01AI175321, and R35GM148231 to S.T. and R01AI173214 to A.H. A.G.W. is supported by NIH training grant T32GM07281. M.S. is supported by training grant NIAID 5T32AI153020. A.G. is supported by the Specialized Training for Advanced Research (STAR) program of the UCLA Department of Medicine and NIH training grant T32AI177290-01. The authors would like to thank the University of Chicago Single Cell Immunophenotyping Core, Animal Resources Center, and UCFlow for providing facilities and equipment.

AUTHOR CONTRIBUTIONS

Conceptualization, S.T., A.G.W., and M.S.; methodology, A.G.W. and M.S.; investigation, A.G.W., M.S., A.G., E.K., B.K., and A.S.; writing – original draft, A.G.W.; writing – review & editing, A.G.W., M.S., A.G., A.H., and S.T.; funding acquisition, S.T. and A.H.; resources, A.H. and S.T.; supervision, S.T. and A.H.

DECLARATION OF INTERESTS

The authors declare no competing interests.

STAR★METHODS

Detailed methods are provided in the online version of this paper and include the following:

- KEY RESOURCES TABLE
- EXPERIMENTAL MODEL AND SUBJECT DETAILS
  - Mouse models
  - Cell lines
- METHOD DETAILS
  - Reagents
  - Induction of endotoxemia
  - Cells
  - Microfluidic device fabrication
  - Microfluidics enabled live-cell imaging
  - Microfluidic stimulation
  - Measurement of bulk RNA-seq expression
  - Measurement of chromatin accessibility using ATAC-seq
- QUANTIFICATION AND STATISTICAL ANALYSIS
  - Image analysis and trace processing
  - Pairwise mutual information analysis
  - RNA sequencing analysis
  - ATAC sequencing analysis
  - Deep learning model construction and validation

SUPPLEMENTAL INFORMATION

Supplemental information can be found online at https://doi.org/10.1016/j.cels.2025.101171.

Received: March 29, 2024
Revised: September 18, 2024
Accepted: January 9, 2025
Published: February 11, 2025

REFERENCES

1. Valls, P.O., and Esposito, A. (2022). Signalling dynamics, cell decisions, and homeostatic control in health and disease. Curr. Opin. Cell Biol. *75*, 102066. https://doi.org/10.1016/j.ceb.2022.01.011.
2. Purvis, J.E., and Lahav, G. (2013). Encoding and Decoding Cellular Information through Signaling Dynamics. Cell *152*, 945–956. https://doi.org/10.1016/j.cell.2013.02.005.

3. Kumar, R., Clermont, G., Vodovotz, Y., and Chow, C.C. (2004). The dynamics of acute inflammation. J. Theor. Biol. *230*, 145–155. https://doi.org/10.1016/j.jtbi.2004.04.044.

4. Son, M., Wang, A.G., Keisham, B., and Tay, S. (2023). Processing stimulus dynamics by the NF-κB network in single cells. Exp. Mol. Med. *55*, 2531–2540. https://doi.org/10.1038/s12276-023-01133-7.

5. Riedemann, N.C., Neff, T.A., Guo, R.-F., Bernacki, K.D., Laudes, I.J., Sarma, J.V., Lambris, J.D., and Ward, P.A. (2003). Protective Effects of IL-6 Blockade in Sepsis Are Linked to Reduced C5a Receptor Expression1. J. Immunol. *170*, 503–507. https://doi.org/10.4049/jimmunol.170.1.503.

6. Bone, R.C. (1996). Immunologic Dissonance: A Continuing Evolution in Our Understanding of the Systemic Inflammatory Response Syndrome (SIRS) and the Multiple Organ Dysfunction Syndrome (MODS). Ann. Intern. Med. *125*, 680–687. https://doi.org/10.7326/0003-4819-125-8-199610150-00009.

7. Sckisel, G.D., Bouchlaka, M.N., Monjazeb, A.M., Crittenden, M., Curti, B.D., Wilkins, D.E.C., Alderson, K.A., Sungur, C.M., Ames, E., Mirsoian, A., et al. (2015). Out-of-Sequence Signal 3 Paralyzes Primary CD4(+) T-Cell-Dependent Immunity. Immunity *43*, 240–250. https://doi.org/10.1016/j.immuni.2015.06.023.

8. Zhang, Q., and Cao, X. (2021). Epigenetic Remodeling in Innate Immunity and Inflammation. Annu. Rev. Immunol. *39*, 279–311. https://doi.org/10.1146/annurev-immunol-093019-123619.

9. Franken, L., Schiwon, M., and Kurts, C. (2016). Macrophages: sentinels and regulators of the immune system. Cell. Microbiol. *18*, 475–487. https://doi.org/10.1111/cmi.12580.

10. West, M.A., and Heagy, W. (2002). Endotoxin tolerance: a review. Crit. Care Med. *30*, S64–S73. https://doi.org/10.1097/00003246-200201001-00009.

11. Foster, S.L., Hargreaves, D.C., and Medzhitov, R. (2007). Gene-specific control of inflammation by TLR-induced chromatin modifications. Nature *447*, 972–978. https://doi.org/10.1038/nature05836.

12. Seeley, J.J., Baker, R.G., Mohamed, G., Bruns, T., Hayden, M.S., Deshmukh, S.D., Freedberg, D.E., and Ghosh, S. (2018). Induction of innate immune memory via microRNA targeting of chromatin remodelling factors. Nature *559*, 114–119. https://doi.org/10.1038/s41586-018-0253-5.

13. Hirohashi, N., and Morrison, D.C. (1996). Low-dose lipopolysaccharide (LPS) pretreatment of mouse macrophages modulates LPS-dependent interleukin-6 production in vitro. Infect. Immun. *64*, 1011–1015. https://doi.org/10.1128/iai.64.3.1011-1015.1996.

14. Maitra, U., Gan, L., Chang, S., and Li, L. (2011). Low-Dose Endotoxin Induces Inflammation by Selectively Removing Nuclear Receptors and Activating CCAAT/Enhancer-Binding Protein δ. J. Immunol. *186*, 4467–4473. https://doi.org/10.4049/jimmunol.1003300.

15. Fu, Y., Glaros, T., Zhu, M., Wang, P., Wu, Z., Tyson, J.J., Li, L., and Xing, J. (2012). Network Topologies and Dynamics Leading to Endotoxin Tolerance and Priming in Innate Immune Cells. PLoS Comput. Biol. *8*, e1002526. https://doi.org/10.1371/journal.pcbi.1002526.

16. Quintin, J., Saeed, S., Martens, J.H.A., Giamarellos-Bourboulis, E.J., Ifrim, D.C., Logie, C., Jacobs, L., Jansen, T., Kullberg, B.-J., Wijmenga, C., et al. (2012). Candida albicans Infection Affords Protection against Reinfection via Functional Reprogramming of Monocytes. Cell Host Microbe *12*, 223–232. https://doi.org/10.1016/j.chom.2012.06.006.

17. Saeed, S., Quintin, J., Kerstens, H.H.D., Rao, N.A., Aghajanirefah, A., Matarese, F., Cheng, S.-C., Ratter, J., Berentsen, K., van der Ent, M.A., et al. (2014). Epigenetic programming of monocyte-to-macrophage differentiation and trained innate immunity. Science *345*, 1251086. https://doi.org/10.1126/science.1251086.

18. Di Luzio, N.R., and Williams, D.L. (1978). Protective effect of glucan against systemic Staphylococcus aureus septicemia in normal and leukemic mice. Infect. Immun. *20*, 804–810. https://doi.org/10.1128/iai.20.3.804-810.1978.

19. Butcher, S.K., O'Carroll, C.E., Wells, C.A., and Carmody, R.J. (2018). Toll-Like Receptors Drive Specific Patterns of Tolerance and Training on Restimulation of Macrophages. Front. Immunol. *9*, 933. https://doi.org/10.3389/fimmu.2018.00933.

20. van 't Veer, C., van den Pangaart, P.S., van Zoelen, M.A.D., de Kruif, M., Birjmohun, R.S., Stroes, E.S., de Vos, A.F., and van der Poll, T. (2007). Induction of IRAK-M Is Associated with Lipopolysaccharide Tolerance in a Human Endotoxemia Model. J. Immunol. *179*, 7110–7120. https://doi.org/10.4049/jimmunol.179.10.7110.

21. Shih, V.F.-S., Kearns, J.D., Basak, S., Savinova, O.V., Ghosh, G., and Hoffmann, A. (2009). Kinetic control of negative feedback regulators of NF-κB/RelA determines their pathogen- and cytokine-receptor signaling specificity. Proc. Natl. Acad. Sci. USA *106*, 9619–9624. https://doi.org/10.1073/pnas.0812367106.

22. Tisoncik, J.R., Korth, M.J., Simmons, C.P., Farrar, J., Martin, T.R., and Katze, M.G. (2012). Into the Eye of the Cytokine Storm. Microbiol. Mol. Biol. Rev. *76*, 16–32. https://doi.org/10.1128/MMBR.05015-11.

23. Kearns, J.D., Basak, S., Werner, S.L., Huang, C.S., and Hoffmann, A. (2006). IκBϵ provides negative feedback to control NF-κB oscillations, signaling dynamics, and inflammatory gene expression. J. Cell Biol. *173*, 659–664. https://doi.org/10.1083/jcb.200510155.

24. Sun, S., and Barreiro, L.B. (2020). The epigenetic encoded memory of the innate immune system. Curr. Opin. Immunol. *65*, 7–13. https://doi.org/10.1016/j.coi.2020.02.002.

25. Oeckinghaus, A., and Ghosh, S. (2009). The NF-κB Family of Transcription Factors and Its Regulation. Cold Spring Harb. Perspect. Biol. *1*, a000034. https://doi.org/10.1101/cshperspect.a000034.

26. Selimkhanov, J., Taylor, B., Yao, J., Pilko, A., Albeck, J., Hoffmann, A., Tsimring, L., and Wollman, R. (2014). Systems biology. Accurate Information Transmission Through Dynamic Biochemical Signaling Networks. Science *346*, 1370–1373. https://doi.org/10.1126/science.1254933.

27. Kellogg, R.A., Tian, C., Lipniacki, T., Quake, S.R., and Tay, S. (2015). Digital signaling decouples activation probability and population heterogeneity. eLife *4*, e08931. https://doi.org/10.7554/eLife.08931.

28. Adelaja, A., Taylor, B., Sheu, K.M., Liu, Y., Luecke, S., and Hoffmann, A. (2021). Six distinct NFκB signaling codons convey discrete information to distinguish stimuli and enable appropriate macrophage responses. Immunity *54*, 916–930.e7. https://doi.org/10.1016/j.immuni.2021.04.011.

29. Son, M., Wang, A.G., Tu, H.-L., Metzig, M.O., Patel, P., Husain, K., Lin, J., Murugan, A., Hoffmann, A., and Tay, S. (2021). NF-κB responds to absolute differences in cytokine concentrations. Sci. Signal. *14*, eaaz4382. https://doi.org/10.1126/scisignal.aaz4382.

30. Wang, A.G., Son, M., Kenna, E., Thom, N., and Tay, S. (2022). NF-κB memory coordinates transcriptional responses to dynamic inflammatory stimuli. Cell Rep. *40*, 111159. https://doi.org/10.1016/j.celrep.2022.111159.

31. Cheng, Q.J., Ohta, S., Sheu, K.M., Spreafico, R., Adelaja, A., Taylor, B., and Hoffmann, A. (2021). NF-κB dynamics determine the stimulus specificity of epigenomic reprogramming in macrophages. Science *372*, 1349–1353. https://doi.org/10.1126/science.abc0269.

32. Rahman, S.M.T., Aqdas, M., Martin, E.W., Tomassoni Ardori, F.T., Songkiatisak, P., Oh, K.-S., Uderhardt, S., Yun, S., Claybourne, Q.C., McDevitt, R.A., et al. (2022). Double knockin mice show NF-κB trajectories in immune signaling and aging. Cell Rep. *41*, 111682. https://doi.org/10.1016/j.celrep.2022.111682.

33. Kull, T., Wehling, A., Etzrodt, M., Auler, M., Dettinger, P., Aceto, N., and Schroeder, T. (2022). NFκB signaling dynamics and their target genes differ between mouse blood cell types and induce distinct cell behavior. Blood *140*, 99–111. https://doi.org/10.1182/blood.2021012918.

34. Kawasaki, T., and Kawai, T. (2014). Toll-Like Receptor Signaling Pathways. Front. Immunol. *5*, 461. https://doi.org/10.3389/fimmu.2014.00461.

35. DeFelice, M.M., Clark, H.R., Hughey, J.J., Maayan, I., Kudo, T., Gutschow, M.V., Covert, M.W., and Regot, S. (2019). NF-B signaling dynamics is

controlled by a dose-sensing autoregulatory loop. Sci. Signal. *12*, eaau3568. https://doi.org/10.1126/scisignal.aau3568.

36. Adamson, A., Boddington, C., Downton, P., Rowe, W., Bagnall, J., Lam, C., Maya-Mendoza, A., Schmidt, L., Harper, C.V., Spiller, D.G., et al. (2016). Signal transduction controls heterogeneous NF-κB dynamics and target gene expression through cytokine-specific refractory states. Nat. Commun. *7*, 12057. https://doi.org/10.1038/ncomms12057.
37. Nakagawa, R., Naka, T., Tsutsui, H., Fujimoto, M., Kimura, A., Abe, T., Seki, E., Sato, S., Takeuchi, O., Takeda, K., et al. (2002). SOCS-1 Participates in Negative Regulation of LPS Responses. Immunity *17*, 677–687. https://doi.org/10.1016/S1074-7613(02)00449-1.
38. Hotchkiss, R.S., Monneret, G., and Payen, D. (2013). Immunosuppression in sepsis: a novel understanding of the disorder and a new therapeutic approach. Lancet Infect. Dis. *13*, 260–268. https://doi.org/10.1016/S1473-3099(13)70001-X.
39. Tong, A.-J., Liu, X., Thomas, B.J., Lissner, M.M., Baker, M.R., Senagolage, M.D., Allred, A.L., Barish, G.D., and Smale, S.T. (2016). A Stringent Systems Approach Uncovers Gene-Specific Mechanisms Regulating Inflammation. Cell *165*, 165–179. https://doi.org/10.1016/j.cell.2016.01.020.
40. Matsumoto, M., and Seya, T. (2008). TLR3: interferon induction by double-stranded RNA including poly(I:C). Adv. Drug Deliv. Rev. *60*, 805–812. https://doi.org/10.1016/j.addr.2007.11.005.
41. Huber, R., Pietsch, D., Panterodt, T., and Brand, K. (2012). Regulation of C/EBPβ and resulting functions in cells of the monocytic lineage. Cell. Signal. *24*, 1287–1296. https://doi.org/10.1016/j.cellsig.2012.02.007.
42. Keenan, A.B., Torre, D., Lachmann, A., Leong, A.K., Wojciechowicz, M.L., Utti, V., Jagodnik, K.M., Kropiwnicki, E., Wang, Z., and Ma'ayan, A. (2019). ChEA3: transcription factor enrichment analysis by orthogonal omics integration. Nucleic Acids Res. *47*, W212–W224. https://doi.org/10.1093/nar/gkz446.
43. Natarajan, A., Yardımcı, G.G., Sheffield, N.C., Crawford, G.E., and Ohler, U. (2012). Predicting cell-type–specific gene expression from regions of open chromatin. Genome Res. *22*, 1711–1722. https://doi.org/10.1101/gr.135129.111.
44. Schmidt, F., Kern, F., and Schulz, M.H. (2020). Integrative prediction of gene expression with chromatin accessibility and conformation data. Epigenetics Chromatin *13*, 4. https://doi.org/10.1186/s13072-020-0327-0.
45. Rahman, S.M.T., Singh, A., Lowe, S., Aqdas, M., Jiang, K., Vaidehi Narayanan, H.V., Hoffmann, A., and Sung, M.-H. (2024). Co-imaging of RelA and c-Rel reveals features of NF-κB signaling for ligand discrimination. Cell Rep. *43*, 113940. https://doi.org/10.1016/j.celrep.2024.113940.
46. Suffredini, A.F., Hochstein, H.D., and McMahon, F.G. (1999). Dose-Related Inflammatory Effects of Intravenous Endotoxin in Humans: Evaluation of a New Clinical Lot of Escherichia coli O:113 Endotoxin. J. Infect. Dis. *179*, 1278–1282. https://doi.org/10.1086/314717.
47. Neupane, A.S., Willson, M., Chojnacki, A.K., Vargas E Silva Castanheira, F., Morehouse, C., Carestia, A., Keller, A.E., Peiseler, M., DiGiandomenico, A., Kelly, M.M., et al. (2020). Patrolling Alveolar Macrophages Conceal Bacteria from the Immune System to Maintain Homeostasis. Cell *183*, 110–125.e11. https://doi.org/10.1016/j.cell.2020.08.020.
48. Kellogg, R.A., Gómez-Sjöberg, R., Leyrat, A.A., and Tay, S. (2014). High-throughput microfluidic single-cell analysis pipeline for studies of signaling dynamics. Nat. Protoc. *9*, 1713–1726. https://doi.org/10.1038/nprot.2014.120.
49. Buenrostro, J.D., Giresi, P.G., Zaba, L.C., Chang, H.Y., and Greenleaf, W.J. (2013). Transposition of native chromatin for multimodal regulatory analysis and personal epigenomics. Nat. Methods *10*, 1213–1218. https://doi.org/10.1038/nmeth.2688.
50. Jetka, T., Nienałtowski, K., Winarski, T., Błoński, S., and Komorowski, M. (2019). Information-theoretic analysis of multivariate single-cell signaling responses. PLoS Comput. Biol. *15*, e1007132. https://doi.org/10.1371/journal.pcbi.1007132.
51. Dobin, A., Davis, C.A., Schlesinger, F., Drenkow, J., Zaleski, C., Jha, S., Batut, P., Chaisson, M., and Gingeras, T.R. (2013). STAR: ultrafast universal RNA-seq aligner. Bioinformatics *29*, 15–21. https://doi.org/10.1093/bioinformatics/bts635.
52. Liao, Y., Smyth, G.K., and Shi, W. (2014). featureCounts: an efficient general purpose program for assigning sequence reads to genomic features. Bioinformatics *30*, 923–930. https://doi.org/10.1093/bioinformatics/btt656.
53. Robinson, M.D., McCarthy, D.J., and Smyth, G.K. (2010). edgeR: a Bioconductor package for differential expression analysis of digital gene expression data. Bioinformatics *26*, 139–140. https://doi.org/10.1093/bioinformatics/btp616.
54. Ritchie, M.E., Phipson, B., Wu, D., Hu, Y., Law, C.W., Shi, W., and Smyth, G.K. (2015). limma powers differential expression analyses for RNA-sequencing and microarray studies. Nucleic Acids Res. *43*, e47. https://doi.org/10.1093/nar/gkv007.
55. Luo, W., and Brouwer, C. (2013). Pathview: an R/Bioconductor package for pathway-based data integration and visualization. Bioinformatics *29*, 1830–1831. https://doi.org/10.1093/bioinformatics/btt285.
56. Raudvere, U., Kolberg, L., Kuzmin, I., Arak, T., Adler, P., Peterson, H., and Vilo, J. (2019). g:Profiler: a web server for functional enrichment analysis and conversions of gene lists (2019 update). Nucleic Acids Res. *47*, W191–W198. https://doi.org/10.1093/nar/gkz369.
57. Langmead, B., and Salzberg, S.L. (2012). Fast gapped-read alignment with Bowtie 2. Nat. Methods *9*, 357–359. https://doi.org/10.1038/nmeth.1923.
58. Li, H., Handsaker, B., Wysoker, A., Fennell, T., Ruan, J., Homer, N., Marth, G., Abecasis, G., and Durbin, R.; 1000 Genome Project Data Processing Subgroup (2009). The Sequence Alignment/Map format and SAMtools. Bioinformatics *25*, 2078–2079. https://doi.org/10.1093/bioinformatics/btp352.
59. Zhang, Y., Liu, T., Meyer, C.A., Eeckhoute, J., Johnson, D.S., Bernstein, B.E., Nusbaum, C., Myers, R.M., Brown, M., Li, W., and Liu, X.S. (2008). Model-based Analysis of ChIP-Seq (MACS). Genome Biol. *9*, R137. https://doi.org/10.1186/gb-2008-9-9-r137.
60. Corces, M.R., Granja, J.M., Shams, S., Louie, B.H., Seoane, J.A., Zhou, W., Silva, T.C., Groeneveld, C., Wong, C.K., Cho, S.W., et al. (2018). The chromatin accessibility landscape of primary human cancers. Science *362*, eaav1898. https://doi.org/10.1126/science.aav1898.
61. Yu, G., Wang, L.-G., and He, Q.-Y. (2015). ChIPseeker: an R/Bioconductor package for ChIP peak annotation, comparison and visualization. Bioinformatics *31*, 2382–2383. https://doi.org/10.1093/bioinformatics/btv145.
62. Castro-Mondragon, J.A., Riudavets-Puig, R., Rauluseviciute, I., Lemma, R.B., Turchi, L., Blanc-Mathieu, R., Lucas, J., Boddie, P., Khan, A., Manosalva Pérez, N., et al. (2022). JASPAR 2022: the 9th release of the open-access database of transcription factor binding profiles. Nucleic Acids Res. *50*, D165–D173. https://doi.org/10.1093/nar/gkab1113.
63. Machlab, D., Burger, L., Soneson, C., Rijli, F.M., Schübeler, D., and Stadler, M.B. (2022). monaLisa: an R/Bioconductor package for identifying regulatory motifs. Bioinformatics *38*, 2624–2625. https://doi.org/10.1093/bioinformatics/btac102.
64. Lawrence, M., Gentleman, R., and Carey, V. (2009). rtracklayer: an R package for interfacing with genome browsers. Bioinformatics *25*, 1841–1842. https://doi.org/10.1093/bioinformatics/btp328.
65. Kocer, E., Ko, T.W., and Behler, J. (2022). Neural Network Potentials: A Concise Overview of Methods. Annu. Rev. Phys. Chem. *73*, 163–186. https://doi.org/10.1146/annurev-physchem-082720-034254.
66. Abadi, M., Agarwal, A., Barham, P., Brevdo, E., Chen, Z., Citro, C., Corrado, G.S., Davis, A., Dean, J., Devin, M., et al. (2016). TensorFlow: Large-Scale Machine Learning on Heterogeneous Distributed Systems. Preprint at arXiv. https://doi.org/10.48550/arXiv.1603.04467.

Please cite this article in press as: Wang et al., Macrophage memory emerges from coordinated transcription factor and chromatin dynamics, Cell Systems (2025), https://doi.org/10.1016/j.cels.2025.101171

STAR★METHODS

KEY RESOURCES TABLE

REAGENT or RESOURCE	SOURCE	IDENTIFIER
Chemicals, peptides, and recombinant proteins		
Ultrapure lipopolysaccharide from E. coli O111:B4	Invivogen	tlrl-3pelps
PAM2CSK4	Invivogen	tlrl-pm2s-1
ODN 1668	Invivogen	tlrl-1668
HMW polyinosinic-polycytidylic acid	Invivogen	tlrl-pic
Murine tumor necrosis factor alpha	R&D Systems	410-MT-010/CF
Murine interleukin 1 beta	R&D Systems	401-ML-010/CF
Murine m-CSF	Peprotech	315-02-10UG
Human fibronectin	R&D Systems	1918-FN
Critical commercial assays		
Macrophage Isolation Kit (Peritoneum), mouse	Miltenyi Biotec	130-110-434
Nextera XT DNA Library Preparation Kit	Illumina	FC-131-1024
NextSeq 500/550 high output kit v2	Illumina	20024906
Deposited data		
RNA seq data reported in this paper	This study	GEO: GSE260996
ATAC seq data reported in this paper	This study	GEO: GSE261647
Single cell NFkB trace data reported in this paper	This study	https://doi.org/10.5281/zenodo.14337874
Experimental models: Organisms/strains		
RelA$^{mVenus/mVenus}$ (C57BL/6)	Adelaja et al..[28] *Immunity*	mVenus-RelA
Software and algorithms		
MATLAB 2023b	MathWorks	http://mathworks.com
R	R Foundation	https://www.r-project.org/
Python	Python	Python.org
Original code	This study	https://doi.org/10.5281/zenodo.14337874

EXPERIMENTAL MODEL AND SUBJECT DETAILS

Mouse models

Endogenously-tagged mVenus-RelA (RelA$^{V/V}$) C57BL/6J mice[28] were housed and bred in specific pathogen free conditions at the University of Chicago or the University of California, Los Angeles. All experiments were performed in accordance with the NIH Guide for the Care and Use of Laboratory Animals and approved by the University of Chicago or UCLA Institutional Animal Care and Use Committees.

Cell lines

Bone-marrow derived macrophages (BMDMs) were differentiated and cultured in RPMI with 10% heat-inactivated FBS (Omega), 1% penicillin/streptomycin (Lonza, Corning), 1% NEAA (Corning), 1% HEPES (Gibco, Corning), 1% sodium pyruvate (Corning), 1% L-glutamine (Fisher, Corning), 0.1% β-mercaptoethanol (Gibco) (complete media) supplemented with 20 ng/mL recombinant murine m-CSF (Peprotech). Isolation and culture described in method details.

Peritoneal macrophages (PMPs) were cultured in complete media. Isolation described in method details.

METHOD DETAILS

Reagents

Ultrapure lipopolysaccharide from E. coli O111:B4 (LPS) (Invivogen), PAM2CSK4 (PAM) (Invivogen), ODN 1668 (CpG) (Invivogen), HMW polyinosinic-polycytidylic acid (polyI:C) (Invivogen), murine tumor necrosis factor alpha (TNFα) (R&D Systems), murine interleukin 1 beta (IL-1β) (R&D Systems), and murine m-CSF (Peprotech) were reconstituted in ultrapure water, aliquoted, and stored at -80C until individual aliquots were used.

Please cite this article in press as: Wang et al., Macrophage memory emerges from coordinated transcription factor and chromatin dynamics, Cell Systems (2025), https://doi.org/10.1016/j.cels.2025.101171

Induction of endotoxemia

6-8 week old male and female RelA$^{V/V}$ mice were injected intraperitoneally with PBS, LPS, or polyI:C at the indicated doses diluted in PBS. Immediately prior to injection and 4, 8, 24, and 48 hours post-injection, weight and core body temperature were recorded. For extraction of peritoneal macrophages, mice were euthanized by CO_2 asphyxiation 4 hours post-injection.

Cells

Bone-marrow derived macrophages (BMDMs) were prepared by culturing bone marrow cells isolated from the femurs and tibias of 6-12 week old male and female RelA$^{V/V}$ mice in complete media supplemented with 20 ng/mL m-CSF. BMDMs were fed on days 2, 4, and 6 with additional complete media supplemented with m-CSF. On day 7-9, adherent BMDMs were washed with PBS and lifted from culture dish with 10 mM EDTA (Fisher) in PBS (Gibco) and either replated in well plates or loaded onto microfluidic devices depending on use.

Peritoneal macrophages (PMPs) were isolated from the peritoneal cavities of 6-8 week old male and female RelA$^{V/V}$ mice by peritoneal lavage with ice cold PBS containing 1% FBS and 2 mM EDTA. PMPs were isolated from the resultant peritoneal cells by negative selection using a Macrophage Isolation Kit (Peritoneum) (Milyenyi) in the MACS MS system (Milyenyi). Peritoneal macrophages were cultured in complete media for subsequent uses.

Microfluidic device fabrication

Silicon wafer master molds for a previously published microfluidic device[29] were used for this study. This device allows independent stimulation of 64 cell culture chambers with any of 14 inputs. Each chamber loads up to 1000 cells. Multilayer polydimethylsiloxane (PDMS) microfluidic device fabrication largely followed previously published protocols.[48] Briefly, 10:1 ratio of PDMS (Momentive) monomer to catalyst was mixed and poured over to form a control layer or spin-coated at 2200 rpm to form a fluid layer, and cured at 80°C. The control layer was cut out and bonded to the fluid layer using oxygen plasma followed by overnight baking at 80°C. Control and input holes were punched, and the device was bonded to a pre-cleaned glass slide using oxygen plasma and baking.

Microfluidics enabled live-cell imaging

Device control valves were connected to electronically actuated pneumatic solenoid valves which can be controlled using a custom graphical interface or pre-written scripts (MATLAB). The device was mounted on an epifluorescence microscope (Nikon) and cell chambers were filled with a 0.2-0.4 mg/mL fibronectin solution (Thermo Fisher, R&D Systems) in PBS overnight. All paths on the microfluidic device were then flushed with complete medium to remove the fibronectin and the live imaging apparatus (Life Imaging Services) was set to 37°C, 5% CO_2, 98% humidity to optimize cell growth conditions. As previously described, BMMPs or PMPs were isolated in suspension, pelleted (5 min, 400 xg), and resuspended at a concentration of 10^7/mL in complete media with phenol red-free RPMI (Gibco) to minimize background fluorescence. Cells were loaded into the microfluidic device and allowed to attach. To stain nuclei for cell tracking 1 hour prior to the start of the experiment, cells were treated with 1 μM Hoechst 33342 in complete media for 5 minutes before washing with complete media. No Hoechst induced cell-death or morphological changes were observed over the 12-16 hours of imaging using the conditions described below. Cells were imaged at 6 minute intervals at 20x magnification using a Nikon Ti2 microscope and images were recorded on a Hamamatsu, ORCA-Flash4.0 V2 camera. Each position was imaged for mVenus-RelA (508-nm, 1 s) and Hoechst (395-nm, 50 ms). No photobleaching or phototoxicity was observed over the course of the imaging process.

Microfluidic stimulation

Previously described reagents were diluted from stock solutions in complete media (supplemented with 20 ng/mL m-CSF for BMMP). Each microfluidic experiment included at least two positive controls (complete media to 10 ng/mL TNFα, 1 ng/mL LPS) and one negative control (complete media only) to ensure comparability and no cross contamination. Ligand doses were chosen to capture 1-1.5 log variation in reagent concentration over a dynamic range of BMMP responsiveness. Ligand were diluted immediately prior to use, stored on ice over the duration of the experiment, and delivered to the device using polyetheretherketone tubing (VICI). Input pressure was maintained at 4 psi to minimize cell shearing during feeding. For cytokine blocking experiments, stimulus A was provided with excess receptor in complete media, followed by stimulus B in complete media without receptor. Other details can be found in our previous published methods.[48] All experiments were done in at least biological duplicate with two independent preparations of cells from different mice on different days.

Measurement of bulk RNA-seq expression

BMMP were replated in 24-well plates at 150,000 cells/well in complete media supplemented with 20 ng/mL m-CSF and allowed to rest overnight. Media was aspirated and Stimulus A in complete media and m-CSF added. After 4 hours, Stimulus A was aspirated and Stimulus B in complete media and m-CSF added. After another 4 hours, stimulus B was aspirated and cells lysed using RLT buffer (Qiagen) + 1% β-mercaptoethanol. RNA was extracted using Dynabeads (Invitrogen), reverse transcription was performed using Maxima HMinus RT (Thermo Fisher) with a poly-dT oligo and a template switching oligo (5' -AA GCAGTGGTATCAACGCAGAGTGAATrGrGrG -3') followed by one cycle of second strand synthesis using KAPA HiFi (Roche, primer: 5'-AAGCAGTGGTATCAACGCAGAGT-3') and purification with Ampure XP beads (Beckman Coulter). Library prep was performed following the Nextera XT procedure. Mean fragment length was between 400-600 bp for each sample. Libraries were sequenced on the NextSeq550 platform (Illumina) using the NextSeq 500/550 high output kit v2.

Please cite this article in press as: Wang et al., Macrophage memory emerges from coordinated transcription factor and chromatin dynamics, Cell Systems (2025), https://doi.org/10.1016/j.cels.2025.101171

Measurement of chromatin accessibility using ATAC-seq

Bone-marrow derived macrophages (BMDMs) were prepared by culturing bone marrow cells isolated from the femurs and tibias of 6-12 week old mice in complete media supplemented with 20 ng/mL m-CSF and fed on 2, 4, and 6 with additional complete media supplemented with m-CSF as described above. On day 7, adherent BMDMs were washed with PBS and lifted from culture dish with 10 mM EDTA (Fisher) in PBS (Gibco) and replated at 7.5X105 cells per well in 6-well plates. The following day BMDMs were stimulated with LPS (1ng/mL), CpG (100nM), polyI:C (1μg/mL), or TNF (10ng/mL) as indicated.

ATAC was performed as preciously described.[49] Briefly, cells were lifted in with Accutase (ThermoFisher) and gentle cell scraping. 5x104 cells were utilized to prepare nuclei. Cells were lysed by using cold lysis buffer at 10mM Tris-HCL pH 7.5, 3mM MgCl2, 10mM NaCl, and 0.1% IGEPAL CA-630. Centrifugation for 10 minutes at 500 × g and suspension in the transposase reaction mixture allowed pelleting of nuclei (25 μl of 2X TD Buffer (Illumina), 2.5 μl of TD Enzyme 1 (Illumina), and 22.5 μl of nuclease-free water). We performed transposase reaction for 30 minutes at 37 °C in a shaker at 800RPM, and purified the fragmented DNA using MinElute PCR purification kit (QIAGEN). These fragments were amplified by PCR to create ATAC-seq libraries (Illumina Nextera sequencing primers were used). Libraries were purified using MinElute PCR kit (by Qiagen). Qubit dsDNA high sensitivity assay kits by Thermo Fisher were used to quantify the libraries, which were then pooled and sequenced on the Illumina NovaSeq SP to generate 50bp paired end reads.

QUANTIFICATION AND STATISTICAL ANALYSIS

Image analysis and trace processing

Images were exported to MATLAB 2021a for processing and single cell analysis using custom code. Flat field and dark frame corrections were applied to images. Individual cell nuclei were segmented using Hoechst images and tracked over successive frames. Background fluorescence was quantified from mean intensity of regions of each image without cells and subtracted from the respective frame. Nuclear segmentation was used to identify median nuclear fluorescence in each frame and normalized to median cytoplasmic fluorescence. The resulting traces were processed to remove cells which undergo death, division, or other sources of error. Cells were tracked with >99% accuracy over up to 8-hour intervals (Video S3)

Each trace was normalized to the mean nuclear/cytoplasmic ratio from the two frames prior to the interval of interest. For BMMPs, AUC was calculated by trapezoidal approximation, and early and late AUC were defined by AUC in the first and last 20 frames (120 minutes). Maximum amplitude was identified by finding the index of maximum amplitude from a smoothed trace (loess method, 3 frame interval, minimum prominence 0.1) to reduce noise, then identifying the nuclear/cytoplasmic ratio for that index in the unsmoothed trace. Peak timing was identified by finding the frame at which a trace first reaches its half-maximal amplitude. For all BMMP experiments, stimulus B (TNF or LPS) AUC and amplitude were normalized to the naïve response to the same stimulus. For PMPs, traces were first smoothed (loess method, 5 frame interval) to reduce the noise due to the small size and movement of PMPs. AUC was calculated by trapezoidal approximation from the smoothed trace and the upper and lower 5% of cells were discarded. No other processing was done unless otherwise noted.

Pairwise mutual information analysis

We used the methods for mutual information calculation developed by Jetka et al.[50] Every other point from the dynamic trace obtained from microscopy were extracted and used as an input for calculation of mutual information. The mutual information *I* between the responses *R* from a pair of samples *S* can be calculated as the difference between the entropy *H* of the entire response (non-conditional entropy) and the sum of entropies from the responses specific to each sample:

$$I(R;\ S)\ =\ H(R)\ -\ H(R|S)$$

I describes the reduction in entropy, or uncertainty, in identifying the sample which a response belongs to due to observing the response. Thus the mutual information can be thought of as representing the ''distinguishability'' between two sample responses. This calculation of mutual information assumes the probability of a response coming from each sample is 0.5 and can vary from 0 (indistinguishable) to 1 bit (entirely distinguishable). Additional information about the calculation of mutual information can be found in the original publication.[50]

RNA sequencing analysis

Adapter trimming and read mapping to the reference genome (GRCm38) was done using STAR with default parameters.[51] Transcript abundance was quantified using the R package featureCounts.[52] Differential gene expression were identified using the R packages edgeR and limma.[53,54] Differential genes (DEGs) were identified compared to naïve macrophages using the cutoffs of Benjamini-Hochberg false discovery rate (FDR) < 0.01 and fold change > 1. Visualization of DEGs in the NF-κB pathway (KEGG: mmu04064) between polyI:C and CpG treatment accomplished using the R package Pathview.[55] We defined synergistic and antagonistic gene regulation by memory in all DEGs using the following equation:

$$\Delta AB_{memory}\ =\ \frac{AB\ -\ (\varnothing+\Delta A\varnothing+\Delta B)}{(\varnothing+\Delta A\varnothing+\Delta B)}$$

Please cite this article in press as: Wang et al., Macrophage memory emerges from coordinated transcription factor and chromatin dynamics, Cell Systems (2025), https://doi.org/10.1016/j.cels.2025.101171

$$\Delta AB_{memory} > 0.25 = Synergy;\ \Delta AB_{memory} < -0.25 = Antagonism$$

Here, we compare the gene expression due to sequential stimulus of ligand A and B (AB) to the expected gene expression if the effects of A and B were independent normalized (the "null hypothesis") by the expected gene expression. The expected gene expression term is shown as the gene expression from naïve, media treated cells (∅) plus the change in gene expression from treatment with ligand A followed by media (ΔA∅) plus the change in gene expression from treatment with ligand B only (ΔB). If ΔAB_{memory} was 25% greater than expected, we considered it synergy, and if ΔAB_{memory} was 25% less than expected, we considered it antagonism.

GO and KEGG overrepresentation analysis on groups of synergistic and antagonistic genes was performed using gProfiler.[56] Enriched TFs were identified using the ENCODE ChIP-seq database in ChEA3.[42]

ATAC sequencing analysis

ATAC-seq reads were aligned to the mm10 genome using bowtie2 version 2.2.5[57] with default parameters except –very-sensitive and –non-deterministic options and were filtered based on mapping score (MAPQ >30) by Samtools version 1.9.[58] Duplicated reads were removed by Picard MarkDuplicates (version 2.18.29). MACS3 (version 3.0.0b1[59]) was used to identify peaks for each sample individually with default settings except FDR of 0.01, -f BAMPE, -g mm, and –nomodel. Peaks from all samples were merged into a single file using iterative overlap peak merging as described in Corces et al.,[60] and all raw peaks quantified using featureCounts.[52] Peaks were normalized, and differentially open chromatin sites compared to media control were identified using edgeR and limma.[53,54] Open peaks were annotated using the R package ChIPseeker[61] and enriched transcription factor binding motifs identified from the JASPAR2022 database[62] using the R package monaLisa.[63] All TFs with logFC enrichment > 1 were considered significant (complete list of enriched TFs can be found in the supplemental information). Genomic tracks were visualized using the R package Rtracklayer.[64]

Deep learning model construction and validation

To evaluate how accurately the deep learning algorithm can evaluate the gene expression changes by the different stimulus sequences and how much information is encoded at different stages of signal transduction, we first sorted data from NF-κB response, RNA-, ChIP-, and ATAC-sequencing and arranged them in a large table. In the table, each row indicates a specific gene in different stimulation condition, while columns contain the data from various measurements and motif analysis. Briefly, in the proximal and distal promoter region of each gene (-1500 to +500 bp from the TSS or -3000 to -1500 and +500 to +3000 bp from the TSS), the three most proximal ATAC peaks were selected and the number of binding motifs for 18 different transcription factors were recorded for each peak. We also included motifs for chromatin regulators which do not interact with specific motifs (EZH2, HDAC, NELFE) which were located in the promoter region. After inclusion of these data from ATAC, ChIP-seq, and motif analyses, the features from NF-κB response dynamics, such as peak height, area-under-curve, and activation time, for each stimulation condition were also evaluated and added to the table. The table now contains multifaceted data from both nucleic and cytosolic measurements, and was used as inputs to a multi-layer perceptron (MLP) neural network.[65] Through this neural network, we linked the arranged inputs to the gene expression changes measured from RNA-sequencing. To enable this, the gene expression data was classified into 4 distinct groups based on the change from the control (fresh medium/fresh medium stimulation). For each gene in each stimulation condition (i.e., for each row entry in the table), if the expression was reduced to less than 0.66 of the control level, it was considered as "downregulated". If the expression was between 0.87 and 1.5-fold of the control, the gene was considered "not significantly changed" by the specified stimulation. Similarly, 3- to 10-fold increase was considered "significantly upregulated", and 20-fold increase or more was "considered highly upregulated." This classification served as an output of neural network, and utilized to evaluate the accuracy of the neural network. We utilized TensorFlow platform to build and optimize the neural network.[66] The constructed MLP network had two or three layers between the input and output layers, where inputs were each row entry from the arranged table and outputs were the 4 classifications based on gene expression changes. The first layer of MLP always had same number of nodes as the number of input variables, while the second or third layer had either half or quarter of nodes from the first layer. After each layer 10% of the connections were dropped, we used ReLu for all activation functions, and 'Adam' method was used for all optimization. To accurately capture the overall performance of the neural network, the 8,894 samples were randomly divided into 5 sub-groups for 5-fold cross-validation. For each train dataset, the best fit MLP model and its prediction for test dataset were evaluated. These predictions from all 5-fold cross-validation were combined into one output column to calculate the accuracy of the overall fitting and model prediction. In other words, for each gene in each condition, we extracted the predicted value of the model only when the gene was used as a test data. After evaluating the accuracy of the model with all data included, we also calculated its accuracy when only subset of input data is used (Figures 7C–7E). These trials with subsets would elicit the correlation between the reactions at specific stage of signal transduction and the gene expression changes. For example, we only used the data from NF-κB translocation dynamics as inputs to neural network to evaluate the mutual information between the cytosolic signal transduction pathway and gene expression output (Figures 7C–7E). Additionally, we used only the TF motif and ATAC data to investigate which TF or combination of TFs has most information about the gene expression changes by the sequential stimulations (Figures 7F and 7G).